Cell Systems

Article

The architecture of binding cooperativity between densely bound transcription factors

Graphical abstract

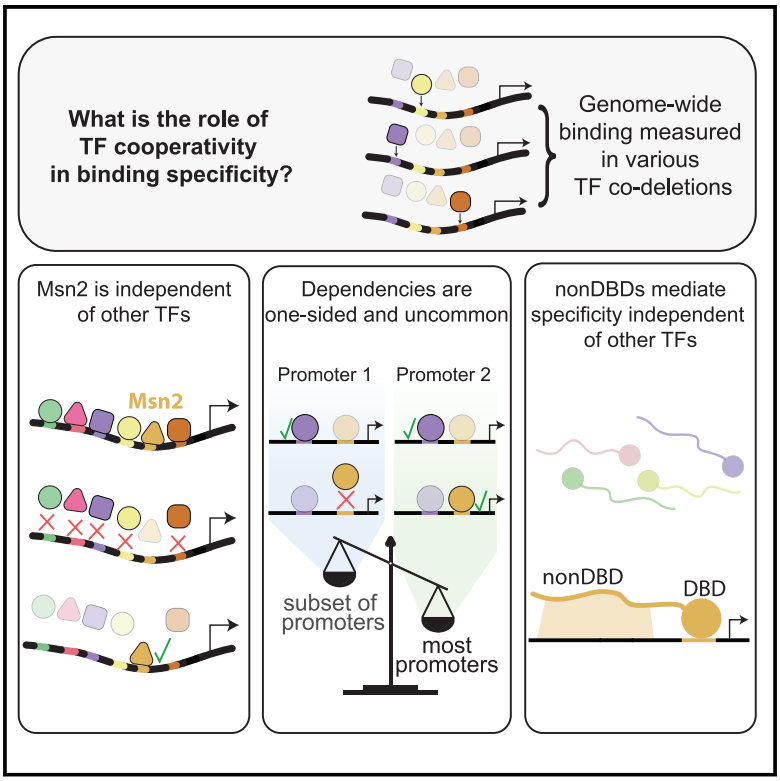

Highlights

- Systematic co-deletion assays examine transcription factor-binding dependencies
- The TF Msn2 allows multiple TF binding at its target promoters
- The binding of Msn2 is invariant to the co-deletion of up to 14 other TFs
- Binding dependencies are uncommon, one-sided, and limited to a subset of promoters

Authors

Offir Lupo, Divya Krishna Kumar, Rotem Livne, Michal Chappleboim, Idan Levy, Naama Barkai

Correspondence

naama.barkai@weizmann.ac.il

In brief

Transcription factors (TFs) bind a subset of their potential sites, which is often attributed to TF cooperativity. Lupo et al. systematically examine binding dependencies by co-deleting multiple TFs and reveal that dependencies are uncommon, one-sided, and cannot account for the role of non-DBD regions in directing binding preferences.

Lupo et al., 2023, Cell Systems *14*, 732–745
September 20, 2023
https://doi.org/10.1016/j.cels.2023.06.010

CellPress

CellPress

Cell Systems

Article

The architecture of binding cooperativity between densely bound transcription factors

Offir Lupo,[1] Divya Krishna Kumar,[1] Rotem Livne,[1] Michal Chappleboim,[1] Idan Levy,[1] and Naama Barkai[1,2,*]
[1]Department of Molecular Genetics, Weizmann Institute of Science, Rehovot 76100, Israel
[2]Lead contact
*Correspondence: naama.barkai@weizmann.ac.il
https://doi.org/10.1016/j.cels.2023.06.010

SUMMARY

The binding of transcription factors (TFs) along genomes is restricted to a subset of sites containing their preferred motifs. TF-binding specificity is often attributed to the co-binding of interacting TFs; however, apart from specific examples, this model remains untested. Here, we define dependencies among budding yeast TFs that localize to overlapping promoters by profiling the genome-wide consequences of co-depleting multiple TFs. We describe unidirectional interactions, revealing Msn2 as a central factor allowing TF binding at its target promoters. By contrast, no case of mutual cooperation was observed. Particularly, Msn2 retained binding at its preferred promoters upon co-depletion of fourteen similarly bound TFs. Overall, the consequences of TF co-depletions were moderate, limited to a subset of promoters, and failed to explain the role of regions outside the DNA-binding domain in directing TF-binding preferences. Our results call for re-evaluating the role of cooperative interactions in directing TF-binding preferences.

INTRODUCTION

Transcription factors (TFs) bind DNA using DNA-binding domains (DBDs) that recognize short sequence motifs. Most motif occurrences in genomes, however, remain unoccupied,[1,2] with TFs with similar motif preferences often selecting different subsets of motif sites.[3,4] This specificity of TF binding presents a fundamental unknown in gene regulation: what distinguishes TF-bound motifs from unoccupied ones? Despite the broad interest and some well-explored cases, the basis of TF-binding specificity remains poorly understood at the genomic scale.[5–8]

DBDs are small, folded domains consisting of ~40–70 amino acids (aa) within the hundreds of TF residues. The remaining non-DBD sequences are enriched with intrinsically disordered regions (IDRs) that lack stable 3D conformations.[9–12] This prevalence of IDRs within TFs suggests a general role in transcription; however, most IDRs remain poorly characterized. Recently, we revealed IDRs that direct TF-promoter selection using multiple weak specificity determinants distributed throughout their sequences,[13,14] and this role received further support.[15,16] The basis of this IDR-mediated binding specificity, however, remains unclear.[6,13,17]

Different models were proposed to explain how TFs select their genomic-binding sites.[6,18] Prevalent among those is cooperative binding,[5,7,8,18–22] whereby two or more interacting TFs co-bind at adjacent motifs. TFs could interact directly through protein-protein interactions (PPIs) or indirectly by affecting nucleosome positioning[7,19,20,23] or DNA structure.[20,24,25] Perhaps, supporting the latter, regulatory regions display rapid motif turnover and rearrangements during evolution,[26–29] which contrasts the stringency of the short composite motifs bound by obligatory TF heterodimers.

Motif combinatorics could provide precise addressing within the genome, which is consistent with the high density of binding sites within regulatory regions.[30] However, proximal sites could serve other purposes, including signal integration or cofactor recruitment following TF binding.[8,31] Well-studied examples supporting TF-binding cooperation exist[32–35]; however, systematic genome-scale analysis of binding cooperativity is largely missing.

In this study, we performed systematic TF co-depletion to examine binding dependencies between two groups of TFs that localize to overlapping promoters (Figure 1A). Unexpectedly, we find no case of cooperative binding. Rather, observed binding dependencies between TFs were unidirectional, moderate, and limited to subsets of bound promoters. Furthermore, those dependencies failed to explain the role of non-DBDs in directing TF-promoter preferences. Our results call for revisiting the role of TF-binding cooperativity in directing binding specificity, and the mechanism through which TFs' non-DBDs contribute to this process.

RESULTS

Multiple TFs localize to promoters bound by the Med15 coactivator

The budding yeast genome encodes for ~150 TFs that regulate specific gene expression.[37] Binding profiles are available for a large fraction of budding yeast TFs from the work of others,[38–40] but individual datasets are partial and difficult to

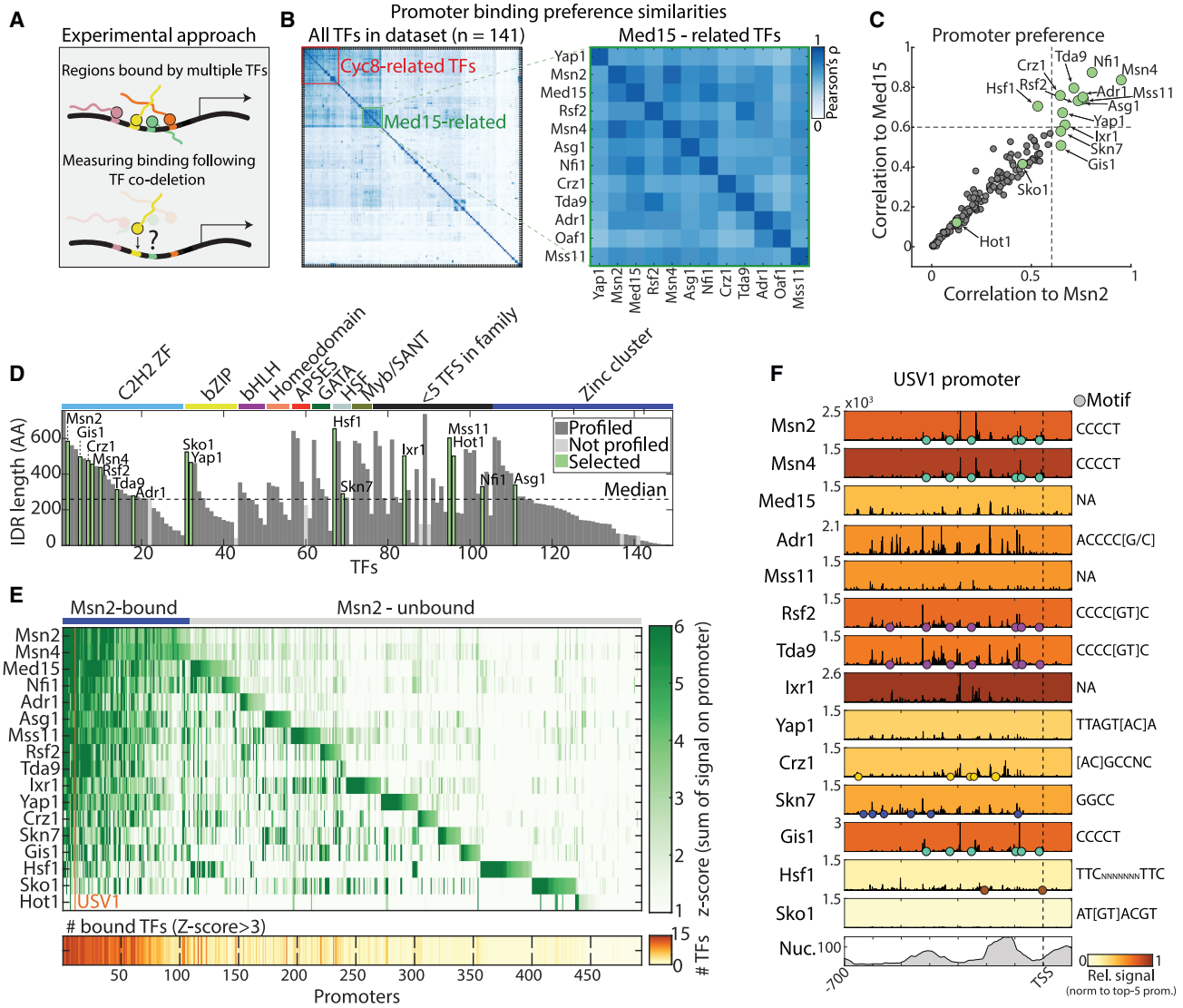

Figure 1. Multiple TFs localize to Med15-bound promoters

(A) *Scheme*: gene regulatory regions contain binding sites for multiple TFs. Cooperative binding by proximally bound TFs can explain TF preferences for localizing to specific subsets of motifs. Co-deleting those TFs can test for cooperativity by distinguishing cooperative binding events that will be lost from the independent ones that will remain.

(B–F) *The pattern of promoter binding overlaps among TFs localizing to Med15-bound promoters*: we used a lab-generated dataset describing TF-binding profiles of 141 (95%) budding yeast TFs (Table S1). Shown in (B) are the promoter-binding preference similarities (measured by Pearson's correlation on the sum of the signal received for each promoter) between all TFs in our dataset, Med15, and Cyc8. The correlation matrix is hierarchically clustered, the two selected TF groups are highlighted, and the Med15-related group is shown in large on the right. The Cyc8-related group is shown in large in Figure S6A. Shown in (C) is the similarity of promoter preferences between each TF and Msn2 (x axis) or Med15 (y axis). TFs chosen for further analysis are highlighted in green. Chosen TFs' family, identity, and IDR length are described in (D; calculated by IUPred2,[36] with values above 0.5 considered disordered). The dashed line indicates the median IDR length across all TFs. TFs within each family are ordered according to IDR length. (E) TF binding to the top-bound promoters by at least one TF in our set. Here, the 100 top-bound promoters by each TF were used and each promoter is shown only once. Msn2-bound promoters are sorted according to the median binding of all TFs, and Msn2-unbound promoters are sorted according to the bound TF. The number of TFs bound to each promoter (*Z* score > 3) is shown below. An example of an Msn2-bound promoter (*USV1*) is indicated in orange. The spread of the signal on it is shown in (F), with the background color indicating the sum of signal on the promoter, normalized to the five top-bound promoters of each TF, circles indicating motif location (sequence shown to the right), and the bottom panel showing nucleosome occupancy.

compare due to differences in profiling methods and growth conditions. To systematically define TFs of overlapping promoter preferences, we used our lab's compendium,[13,14,41,42] which includes binding profiles for 141 (95%, Table S1) TFs, all acquired using chromatin endogenous cleavage with high-throughput sequencing (ChEC-seq[43]) in cells subjected to partial nutrient deprivation (OD_{600} = 4). Overall, ChEC-seq profiles were of high spatial resolution (Figures S1A–S1C) and differed greatly from that of free-MNase (Figure S1D). To our knowledge, this dataset includes all TFs with stress-related functions.

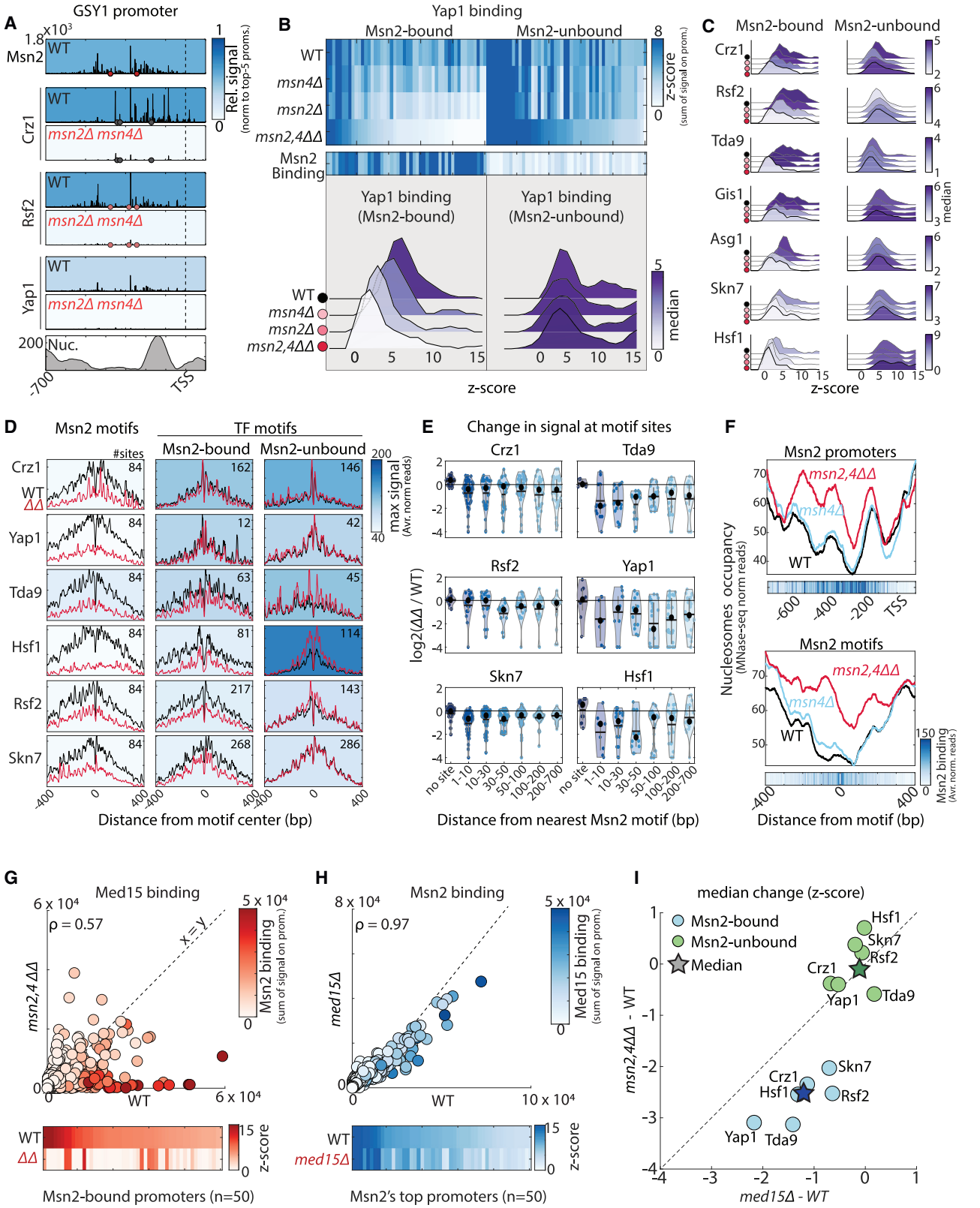

Figure 2. Msn2/4 are required for the binding of multiple TFs at Msn2-bound promoters

(A–C) *Msn2/4 deletion abolishes TF binding at a subset of promoters*: (A) Shown is the binding of the indicated TFs at the Msn2-target promoter *GSY1* in wild-type and Msn2/4 deletion backgrounds (notation as is Figure 1F). (B) Yap1 binding to its target promoters which are either bound or unbound by Msn2 within the

(legend continued on next page)

The majority of TFs localize within a subset of ~1000 (~20%) promoters[38] that display fuzzy nucleosome organization[44–46] and associate mostly with stress or poor-nutrient adaptation. To define TF candidates for binding cooperativity, we clustered the promoter preference similarities between all TFs, revealing two prominent groups (Figure 1B). One of those included stress-related TFs together with the coactivator Med15, a mediator tail subunit that interacts with most budding yeast TFs,[47–49] whereas the second included the general Cyc8 corepressor together with its recruiting TFs.[50] Focusing on the first cluster, we noted that Med15 binding was highly similar to that of the Msn2/4 paralogs[42,51,52] (Pearson's ρ = 0.86 and 0.84, respectively, comparing promoter preferences, Figures 1B and S1D). Msn2 binding preferences depend on its non-DBD,[13] rendering it a promising candidate for cooperative binding.[22] We therefore selected a group of 14 TFs, including 12 that showed the highest similarity (correlation) with either Med15 or Msn2 ($\rho > 0.6$) and 2 (Sko1 and Hot1) previously implicated in Msn2-related transcription[53] (Figure 1C). Seven of the selected TFs were of the zinc-finger (C2H2 ZF) family, and most contained long and disordered non-DBDs (IDR content of 278–654 aa, Figure 1D). Motif preferences observed in our data agreed well with previous *in vitro* or *in vivo* studies[3,54,55] (Figure S1E). As expected, only subsets of motif occurrences were occupied (Figure S1F).

Collecting all promoters bound by the selected TFs revealed dense TF binding at Msn2-preferred promoters (Figures 1E and 1F). Accordingly, those promoters included not only the Msn2 motif but also motifs of the additionally bound TFs (e.g., *USV1*, Figures 1F and S1G). This high overlap in promoter binding rendered the selected TFs promising candidates for cooperative binding.

Msn2/4 facilitates the binding of multiple TFs at their target promoters

We began our analysis by examining whether Msn2 facilitates the binding of other TFs. Deleting Msn2 or its paralog Msn4 individually had a small effect, but co-deletion of both reduced the binding of multiple TFs to most Msn2-bound promoters (Figures 2A–2C). Of note, this effect was specific, as TF binding to promoters lacking Msn2 was unaffected (Figures 2B and 2C). To examine whether the Msn2 non-DBD is sufficient for TF recruitment, we fused it to the strong Rpn4-DBD,[13] shifting its localization to a new subset of promoters (Figure S2A). None of the six tested TFs (nor the intact Msn2) was recruited to those new promoters (Figures S2B and S2C). We conclude that Msn2/4 are required, but not sufficient, for multiple TF-promoter associations.

To further examine the dependency of the tested TFs on Msn2/4, we examined bindings around motif sites (Figures 2D and S2D). This revealed that all tested TFs localized to their own motifs while also showing a significant preference for the Msn2 motif at its bound promoters. Notably, Msn2/4 deletion reduced TF preference to not only Msn2 motifs but also its self-motifs, when those appear in Msn2-bound promoters. Furthermore, classifying individual binding sites based on their distances from the nearest Msn2 site revealed that the effect of Msn2/4 deletion extended across the promoter region (Figure 2E). This effect was also manifested at the nucleosome level, as Msn2/4 deletion increased nucleosome occupancy at Msn2-bound promoters, reaching considerable distances from Msn2/4 binding sites (Figures 2F and S2E). We conclude that Msn2/4 influence on TF binding extends beyond their immediate proximity, spanning hundreds of bases around their binding sites.

The binding of the coactivator Med15 was also lost from Msn2-bound promoters in the Msn2/4-deleted strain (Figure 2G). Med15 interacts with most TFs' activation domains[49] and could therefore mediate the long-range effect of Msn2/4.[22] To test this, we mapped the binding of six Msn2/4-recruited TFs in Med15-deleted cells. Msn2 binding profile remained insensitive to this deletion (Figure 2H), as we previously reported.[13] Other TFs were affected, with Yap1 showing the most significant loss

indicated backgrounds. Promoters are ordered by Yap1 binding in Msn2/4-deletion, and Msn2 binding is shown below. The distributions of binding intensities for Yap1 are shown at the bottom, and their color indicates their median. *Z* score values larger 15 were assigned as 15. The effect of Msn2 and Msn4 deletion on seven additional TFs is depicted in distributions of the binding signal at Msn2/4-bound and Msn2/4-unbound promoters is shown in (C), notation as in (B). Note the specific reduction in binding from Msn2-bound promoters, while Msn2-unbound promoter are mostly unaffected (or show a relative increase in signal).

(D) *Multiple TFs show preferential localization to the Msn2/4 motif, which is lost upon Msn2/4 deletion*: shown is the average binding signal of the indicated TFs around Msn2 motifs (left) and at its own motifs (right), distinguishing Msn2-bound or unbound promoters, and comparing wild-type and Msn2/4-deleted backgrounds. Only motif sites within the respective TF-bound promoters are included. The number of motif occurrences within the respective promoters is shown at the top-right, and the background color indicates the maximal signal. An example of the raw binding signal around these sites is shown for Crz1 in Figure S2D.

(E) *The effect of Msn2/4 deletion extends to hundreds of bases away from Msn2 sites*: shown is the change in signal between Msn2/4 deletion to wild-type backgrounds for the indicated TFs at individual binding sites, classified according to the nearest Msn2-bound site. Only sites within each TFs' top-bound promoters (in wild-type background) are shown. Values lower than -4 (in $\log_2$ scale) were set to be -4. Note that for all TFs, sites with no adjacent Msn2 site are unaffected by Msn2/4 deletion, while sites near an Msn2 site show reduced signal, even at distances larger than 200 bps. The median and mean of each class are indicated by a black circle and a bar, respectively.

(F) *Msn2/4-deletion increases nucleosome occupancy within their target promoters*: shown is the average nucleosome signal (measured by MNase-seq) across Msn2/4-bound promoters centered at their TSS (top) or at Msn2/4 top-bound motifs, ordered according to nearest TSS (bottom), in wild-type, Msn4-deletion, and Msn2/4-deletion backgrounds. The average Msn2 binding signal is shown below. For control, a similar analysis was done on a different set of promoters and motifs (Figure S2E).

(G and H) *Msn2/4 deletion abolishes Med15 binding at Msn2-bound promoters, while Msn2 binding is invariant to Med15 deletion*: shown are scatter plots comparing Med15 promoter binding at Msn2/4-deleted vs. wild-type backgrounds (G) and Msn2 promoter binding in Med15-deleted and wild-type backgrounds (H). Each dot represents the sum of signal (normalized reads) on each promoter, color indicates the sum of signal of Msn2 (red) or Med15 (blue). Pearson's correlation of promoter preferences is indicated on top. The binding on Msn2-bound promoters is shown below in *Z* scores.

(I) *Med15 partially explains the effect of Msn2/4 on TF binding*: shown on top is the median change in binding of the indicated TFs to Msn2-bound and unbound promoters in the indicated backgrounds. Note that the reduced binding signal upon Med15-deletion is lower than that observed upon Msn2/4 deletion and occurs specifically at Msn2-bound promoters. The median across all TFs is indicated with a star. The change in binding at individual promoters is shown in Figure S2G.

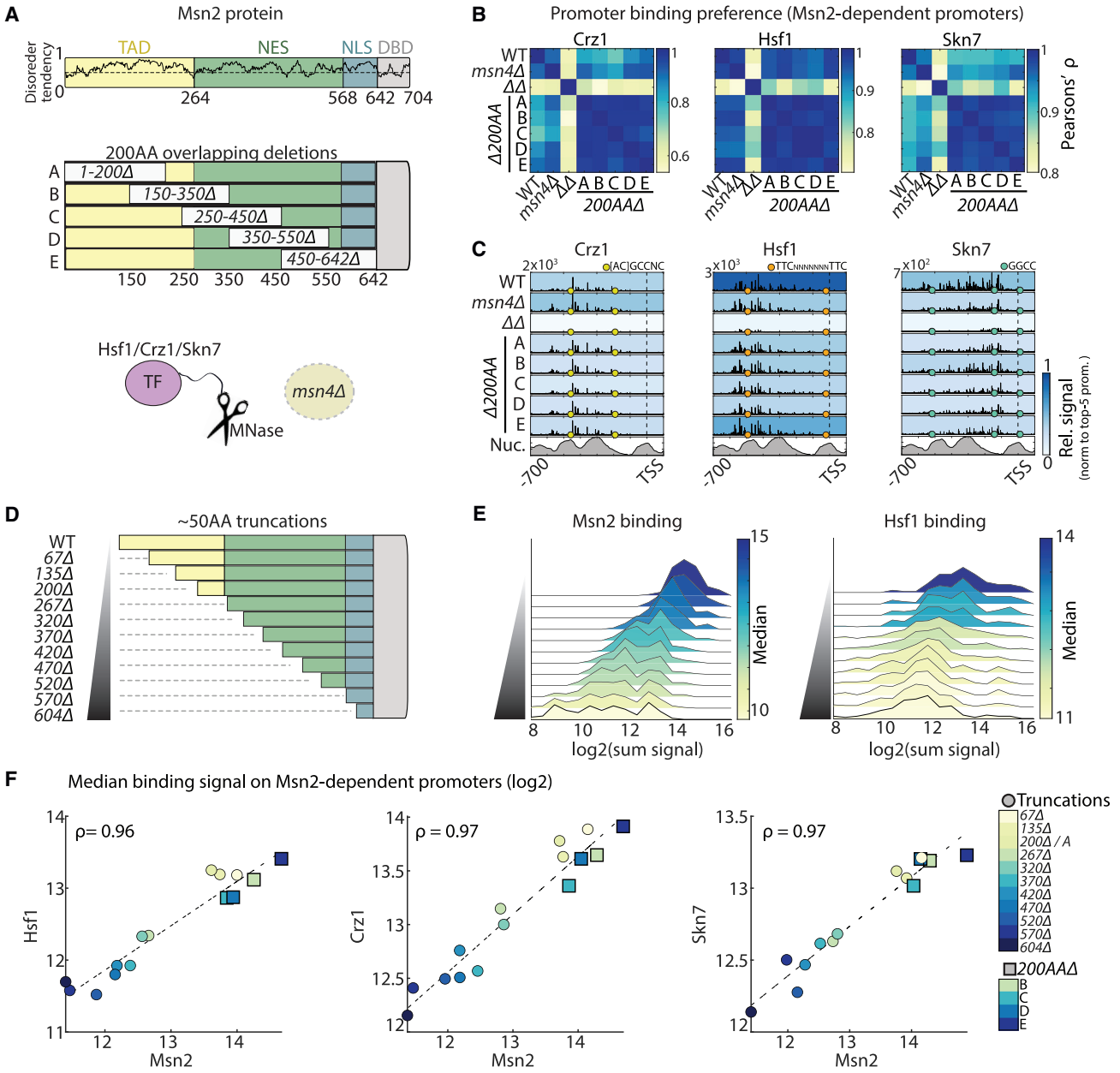

Figure 3. Msn2 enables TF binding at its target promoters using the same multiplicity of weak sequence regions guiding its own binding

(A–C) *No specific 200 aa region within Msn2 is required for allowing TF binding at Msn2-bound promoters*: binding of the indicated TFs was measured in Msn4-deleted strains expressing an Msn2 variant deleted of the indicated 200 aa (scheme in A, note Msn2 disorder tendency on top). (B) Similarities of promoter-binding preferences for each TF on Msn2-dependent promoters (promoters bound by Msn2 and the indicated TF which are lost upon Msn2/4-deletion) between the indicated backgrounds. Note that TF preferences remain largely insensitive to the various 200 aa deletions. This general pattern is exemplified by plotting the respective binding signal along the *UGP1* target promoter (C), notation as in Figure 1F.

(D and E) *Msn2 truncations lead to a gradual loss of TF binding at Msn2-bound promoters*: TF binding was measured in Msn4-deleted strains expressing the indicated Msn2 truncation variant (D). Distributions of Msn2 and Hsf1 promoter-binding signal (sum of signal on promoters) are shown in (E). Note the gradual change in Msn2 and Hsf1 binding at Msn2-bound promoters.

(F) *Msn2 truncations exert proportional effects on the binding of Msn2 and Msn2-dependent TFs*: median promoter-binding signal of Msn2 and the indicated TFs to Msn2-dependent promoters. Each dot represents an Msn2 variant, color-coded as indicated. Differences in binding on individual promoters are shown in Figures S3C and S3D.

(Figures 2I, S2F, and S2G). However, the effects of Med15 deletion were moderate and lower than those of Msn2/4 deletion (Figures 2I and S2F). In particular, TF preferences for the Msn2 motif were retained (Figure S2H). We conclude that Med15 plays a partial (direct or indirect) role in transducing the long-range contribution of Msn2 to TF-promoter binding.

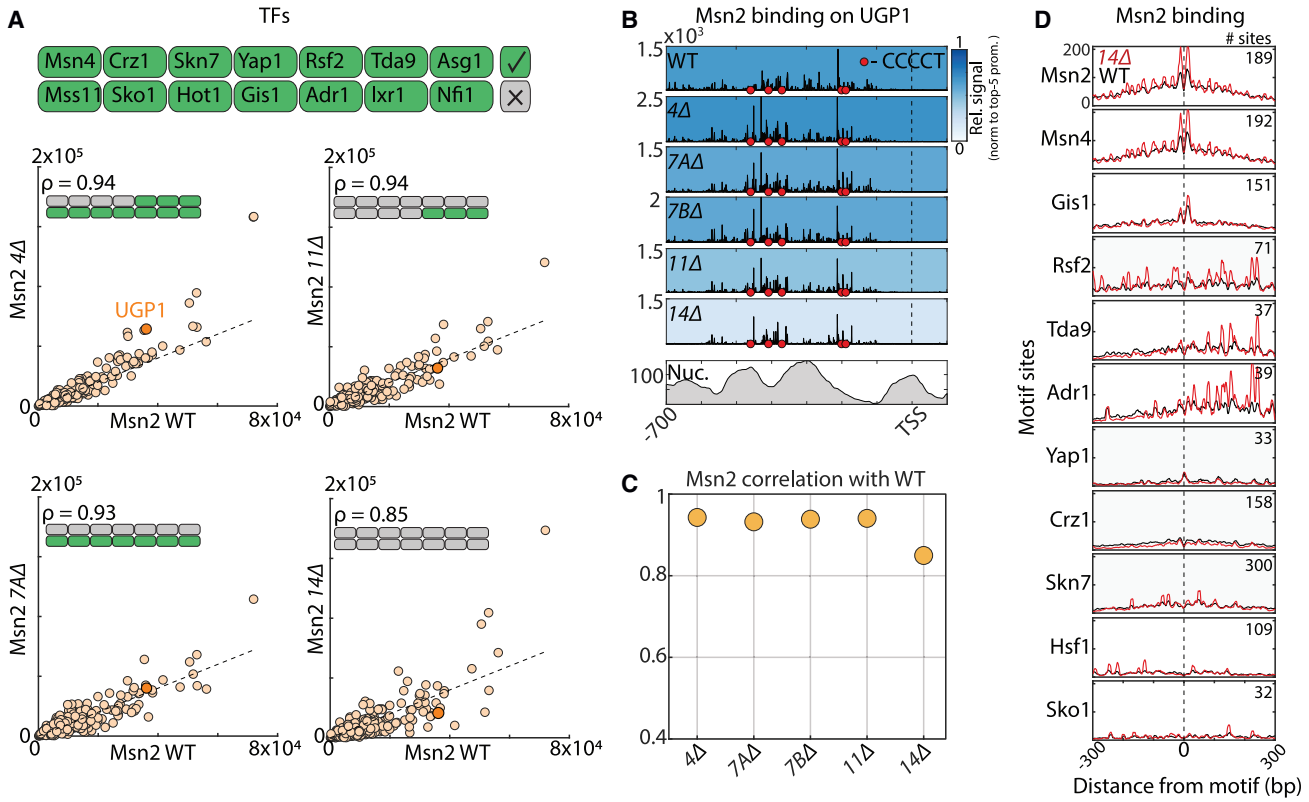

Figure 4. Msn2 recognizes its promoters independently of other TFs

(A–C) *Msn2 retains binding at its target promoters upon co-deletion of other TFs localizing to its promoters*: shown in (A) are the promoter-binding preferences of Msn2 in wild-type and TF co-deletion backgrounds. Each dot represents the total signal on a promoter. The deleted TFs are indicated on top (gray). Also shown is the binding of Msn2 along a representative promoter (B, notation as in Figure 1F) and the overall similarities (Pearson's correlation) of Msn2 promoter preferences between the indicated TF co-deletion and wild-type backgrounds (C).

(D) *Msn2 shows no preference for motifs bound by its proximal-bound TFs*: shown is the average Msn2 binding signal around motif sites of each deleted TF in wild-type (black) and 14 TF co-deletion (red) backgrounds. Only motifs found in the top 100-bound promoters of each TF were included. y axis limits are the same for all panels, according to the upper panel.

Msn2 truncations gradually reduce TF recruitment in proportion to the gradual loss of binding by Msn2 itself

Our results revealed that Msn2 is needed to allow the binding of multiple TFs at its target promoters. We next examined Msn2 region(s) causal for this recruitment. In this, we were interested in whether Msn2 recruits all TFs through the same regions, and whether those regions correspond to the (few) structural segments within its disordered non-DBD (Figure 3A). We examined that by profiling the binding of the recruited TFs in strains devoid of Msn4 and carrying a truncated Msn2, searching for variants that abolish TF recruitment.

As a first set of Msn2 variants, we deleted 200-aa segments, covering the full Msn2 non-DBD (Figure 3A). We previously showed that Msn2 binding is invariant to those deletions,[13] and we verified this in the Msn4-deleted strains (Figure S3A). Unexpectedly, the binding of the tested TFs was also invariant to those truncations (Figures 3B and 3C). Therefore, no 200-aa region within Msn2 is individually necessary for TF recruitment.

To examine for redundant regions, we generated a series of truncations in which we gradually shortened Msn2 through sequential ~50-aa deletions (Figure 3D). We previously found those truncations to gradually shift Msn2-binding preferences,[13] and we verified this now in Msn4-deleted strains (Figure S3A). Notably, promoter binding by the tested TFs followed the same gradual dynamics, independent of TF identity (Figures 3E, 3F, and S3B–S3D). We conclude that Msn2-mediated TF recruitment scales with Msn2 promoter occupancy and is accordingly dependent on the cumulative action of multiple weak determinants distributed throughout its non-DBD.

Msn2 localizes to its preferred promoters independently of other TFs

Our results, showing a coordinated loss in promoter binding by Msn2 and its recruited TFs, are consistent with models of cooperative binding, predicting that Msn2 binding will be similarly lost when deleting its interacting TFs. To examine that, we mapped Msn2 binding in strains co-deleted of Msn4 and three TFs showing pronounced Msn2/4 dependence (*msn4Δ*, *crz1Δ*, *skn7Δ*, and *yap1Δ*). Msn2 binding preferences, however, remained invariant to those deletions, as can be appreciated from the overall similarity of promoter preferences (ρ = 0.94, Figures 4A–4C) or binding at individual promoters (e.g., *UGP1*, Figure 4B). Note that to control for possible changes in Msn2 abundance among mutants, we expressed Msn2 using a constitutive promoter of similar expression

levels, which had no detectable effect on Msn2 binding (ρ = 0.98, Figure S4A).

Given this invariance of Msn2 binding preferences to this four TF co-deletion, we deleted three additional TFs (*rsf2Δ*, *tda9Δ*, *asg1Δ* or *mss11Δ*, *sko1Δ*, *hot1Δ*), generating two strains, each deleted of seven TFs. Again, Msn2 binding pattern was hardly affected (ρ = 0.93–0.94 with wild-type profile, Figures 4A–4C). Next, we combined all deletions and added Gis1, co-deleting 11 TFs (*msn4Δ*, *crz1Δ*, *skn7Δ*, *yap1Δ*, *rsf2Δ*, *tda9Δ*, *asg1Δ*, *mss11Δ*, *sko1Δ*, *hot1Δ*, *gis1Δ*). Still, Msn2 binding remained largely invariant (ρ = 0.94, Figures 4A–4C), as was its paralog Msn4 (ρ = 0.88, Figure S4B).

Finally, we added three more deletions (*adr1Δ*, *ixr1Δ*, *nfi1Δ*). This massive 14-TF deletion slowed the growth rate by ∼40% (Figures S4C and S4D); however, Msn2 binding preferences were only moderately affected (ρ = 0.85; Figures 4A–4C). Of note, even in this strain, Msn2 retained binding at most of its target promoters, although the relative binding strength was reduced (Figure S4E). The binding pattern of Msn2 across the promoter remained largely unaffected by the TF deletions (Figure S4F). Consistently, although Msn2 localized preferentially to its own motif, it showed no preference for motifs of the other tested TFs (Figure 4D). In addition, deleting the last 3 TFs individually had no effect on Msn2 binding preference (Figure S4G). We conclude that Msn2 recognizes its target promoters largely independent of its neighboring TFs, including those it effectively recruits to those same promoters.

Beyond Msn2/4-bound promoters, TF binding shows limited dependency on neighboring TFs

We next used our strains lacking the tested TFs to systematically examine for binding dependencies among them. For this, we profiled the binding of seven TFs in cells co-deleted of 11 TFs (including Msn2/4), again replacing their promoters with a constitutive one to limit potential changes in abundance (Figure S5A). Focusing first on Msn2/4-bound promoters, we noted that most Msn2/4-independent binding events were retained in the 11 TF co-deleted strains (Figure 5A). Furthermore, re-introducing Msn2 fully rescued TF (and Med15) binding to Msn2-bound promoters in all tested cases (Figure 5B). Of note, Msn2 did not rescue the increased nucleosome occupancy at those promoters (Figures 5C and S5B), suggesting that nucleosome loss is the result, rather than the cause of TF binding. We conclude that Msn2/4 fully account for TF-binding dependencies within their bound promoters.

When tested across all promoters, TF-binding preferences within the 11 TF co-deletion strains were somewhat shifted with respect to the Msn2/4 deleted strains (Figure 5D, ρ = 0.77–0.96), although all TFs, including the moderately affected ones (Yap1 and Tda9; ρ = 0.83, 0.77) retained binding to their top targets (Figures 5A and S5C). To define the dependencies explaining those additional effects, we examined the average TF binding around different motifs at TF-bound promoters (Figure 5E). Three cases indicating unidirectional dependencies emerged, including the known recruitment of Yap1 by Skn7.[56] The two additional ones predicted the recruitment of Tda9 and Yap1 by Crz1, which we verified through Crz1 deletion (Figure 5F). These dependencies were one-sided, as neither Skn7 nor Crz1 showed similar TF-dependent motif localization. We conclude that binding dependencies within the selected TF group are unidirectional and, besides Msn2/4, are of limited effect.

Transcription repressors of overlapping binding preferences show limited binding cooperativity

We extended our study to the second group of similarly bound TFs, which included the general corepressor Cyc8[50,57] (Figure S6A). Thirty of the 141 TFs in our compendium showed high similarity to Cyc8 (ρ > 0.6), including 11 TFs known to interact with the respective Tup1-Cyc8 complex (Figure 6A; Table S1). We selected 15 of the top-correlating ones and added Yap4 and Rgt1, previously implicated in Tup1-Cyc8 recruitment.[58,59] The selected TFs were of diverse families, displayed varying lengths and IDR content, and were localized to overlapping promoters (Figures 6B and S6A). For all TFs in this group, motif preferences derived from our data agreed well with the known preferences defined in previous *in vitro* or *in vivo* studies[3] (Figure S6B).

As Cyc8 interacts with most TFs in this group, we asked whether it affects their promoter binding. Due to the severe growth defects caused by Cyc8 deletion, we examined this through rapid Cyc8 depletion using auxin-inducible degron[60] (Figure S6C). All five tested TFs retained their binding preferences upon Cyc8 depletion (ρ = 0.87–0.92, Figures S6D and S6E), suggesting that Cyc8 itself has no significant effect on TF binding.

We next generated strains deleted of combinations of six, twelve, or sixteen TFs from the Cyc8-correlated group and examined the consequences on TF binding (Figures 6C–6E). Although some TFs were highly sensitive to those massive deletions (e.g., Rox1 and Nrg1/2), most TFs were only moderately affected (e.g., Sok2 and Ixr1, Figures 6C–6E). The binding of Cyc8 itself was lost from a subset of promoters but, perhaps unexpectedly, was retained and even strengthened in others (ρ = 0.81, Figure S6F). Of note, the binding of Msn2, measured as well in this TF co-deletion background, was hardly affected (ρ = 0.92, Figures S6G and S6H).

To define the structure of binding dependencies among the Cyc8-related TFs, we examined the average TF binding around the various motifs. Each of the tested TFs localized to its known motifs, and most TFs retained this localization also in the TF co-deleted strains (Figure 6F). Exceptions include TFs that lost (e.g., Nrg1/2, Mig1) or gained (e.g., Rox1, Mot3) motif binding signal. Furthermore, most TFs did not localize to motifs of other TFs, consistent with the low effects of the TF co-deletions (Figure 6G). Nrg1/2 were again exceptions, showing preferred localization at Sko1 and Mot3 sites, which was reduced in the deletion strains. Those effects were again unidirectional, as neither Sko1 nor Mot3 localized to Nrg1/2 sites or showed reduced abundance around those sites in the deletion strain. This analysis further predicted unidirectional dependencies of Mig1 on its similarly bound paralogs Mig2/3 and Rgt1 (Figure 6G), which we verified using single TF deletions (Figure 6H). Overall, interactions in this TF group appeared less frequent than in the Med15 group, in line with the previously noted synergism among transcriptional activators.[8,61] We conclude that within our set of tested TFs, cases of TF-binding dependencies are limited and, when exist, are unidirectional and affect only a subset of promoters.

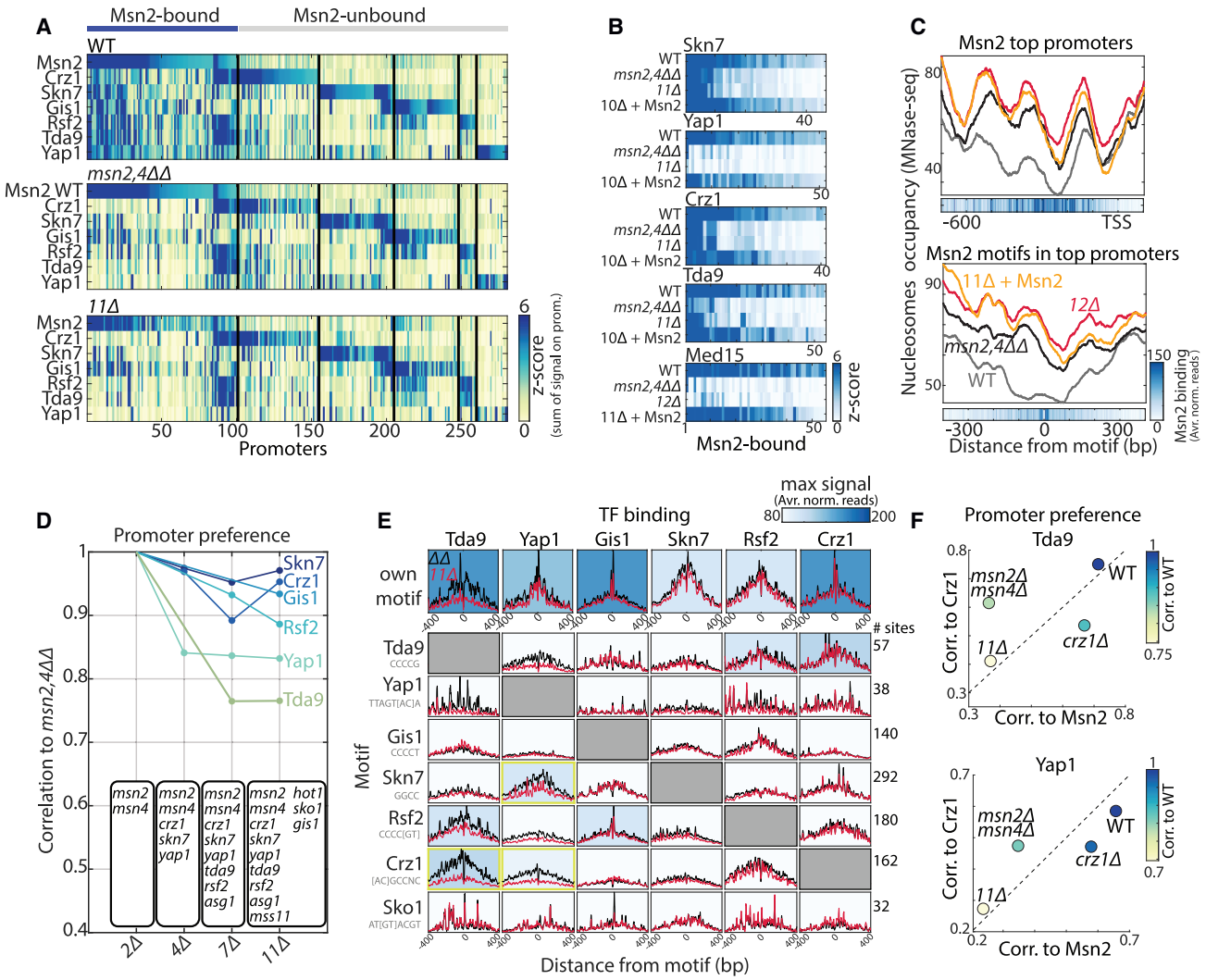

Figure 5. TF-binding dependencies are infrequent and one-sided

(A) *Msn2 accounts for all binding dependencies at Msn2-bound promoters*: shown is the binding of the indicated TFs within wild-type (top), Msn2/4-deletion (middle), and 11 TF co-deletion (bottom) backgrounds. The deleted TFs are listed in (D). All promoters bound by at least one the indicated TFs in the wild-type background were included. Each promoter group (top-bound promoters of a given TF) was clustered using k-means in the co-deletion background, and their order was kept between plots.

(B and C) *Msn2 is sufficient to rescue TF localization to Msn2-bound promoters, but not nucleosome eviction*: shown in (B) is the binding of the indicated TFs (and Med15) to Msn2-dependent promoters in the indicated backgrounds. Note that Msn2 is sufficient to restore the binding of all measured TFs and Med15 to its target promoters. The deleted TFs are listed in (D). (C) Shown is the nucleosome pattern at Msn2 top-bound promoters and around Msn2 motifs in these promoters (notation as Figure 2F).

(D) *Beyond Msn2/4, TFs show limited dependencies*: shown are the similarities (Pearson's correlation) in promoter-binding preferences between Msn2/4-deleted and the indicated backgrounds. Note that, with the exception of Yap1 and Tda9, all TFs retain a high correlation ($\rho > 0.88$) to Msn2/4-deletion. See Figure S5C for a comparison to wild-type background.

(E and F) *Motif localization points at one-sided TF-binding dependencies*: shown in (E) is the average binding of the indicated TFs around their preferred motifs (top) and around motifs of other TFs (bottom). Only motifs located within bound promoters are included, and the binding signal is compared between Msn2/4-deletion (black) with 11 TF co-deletion (red) strains. The background color indicates the maximal signal. Note the co-localization of Tda9 and Yap1 to Crz1-motifs, which is lost in the 11 TF co-deletion background, reflecting the preferential loss of Tda9 binding from Crz1-bound promoters. (F) Single-deletion of *CRZ1* validates binding dependencies: shown is the correlation in promoter-binding preference for Tda9 (top) and Yap1 (bottom) at the indicated backgrounds to Msn2 (x axis) and Crz1 (y axis). The color indicates the correlation to wild-type background. Note the differential dependency on both Crz1 and Msn2/4.

TF non-DBDs direct binding specificity independent of TF interactions

Our data above testing systematically for dependency among similarly bound TFs show no evidence for cooperative TF binding but still describes multiple unidirectional dependencies. We therefore asked whether those dependencies explain the role of non-DBDs in directing TF-binding locations[13,14] (Figure 7A). For 11 of our tested TFs, binding preferences of DBD-only

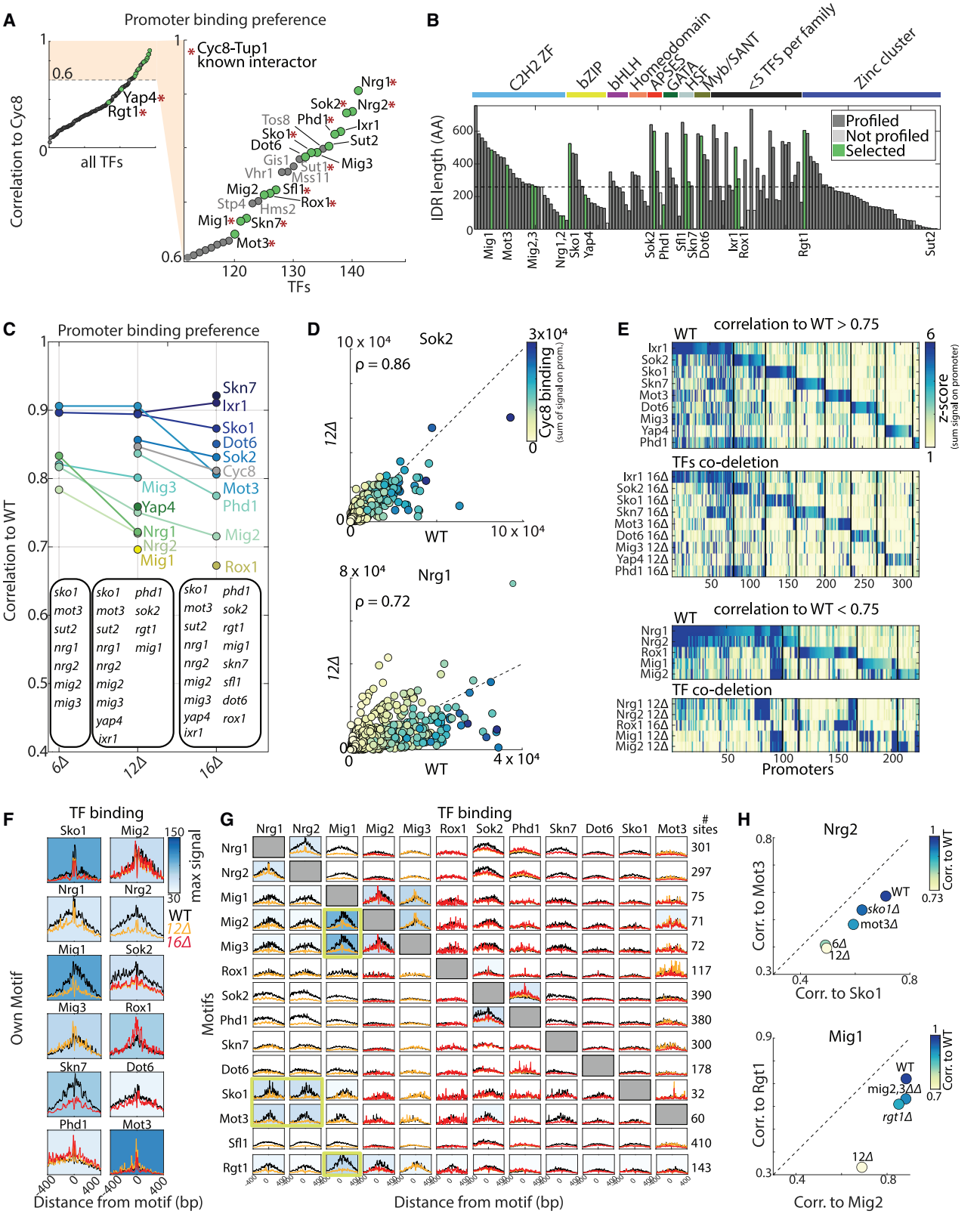

(legend on next page)

mutants (lacking most of their non-DBD) were mapped[14] and, in all those cases, differed from those of full TFs (Figure S7A), displaying reduced binding signal at some TF-bound promoters as well as gain of binding at new promoters (exemplified by Sko1, Figure 7B).

Comparing the changes in binding profiles of DBD-only variants or TF co-deletions revealed little similarities (Figures 7C and 7D). Specifically, TF co-deletion did not increase binding at DBD-only-unique promoters, nor did it reduce binding at non-DBD-dependent promoters (Figures 7C and S7C). Exceptions included Yap1 and Mig1, although also in those cases, TF-binding preferences within the TF co-deletion were better correlated with those of full TF than with the DBD-only variant (Figure 7D). We conclude that within our set of tested TFs, direct interactions fail to explain the role of non-DBDs in directing binding preferences.

DISCUSSION

Cooperative DNA binding by interacting TFs presents a compelling explanation for the challenge of binding specificity. Two necessary conditions for this model are satisfied. First, at the level of the DNA, regulatory sequences contain closely spaced motifs bound by multiple TFs. Second, at the level of TFs, regions outside the DBD play a prominent role in directing DNA binding, potentially by interacting with other TFs. Still, functional evidence confirming the role of TF co-binding in directing binding specificity was limited to specific cases. Our study suggests that cooperative binding is rather infrequent and, contrasting the prevailing notion, fails to explain the specificity of TF binding.

We analyzed possible interactions among 28 TFs that form two hubs within the co-localization network of budding yeast TFs. Selecting those TFs as candidates for cooperative binding was motivated not only by their high binding overlap but also by the prominent roles of their non-DBDs in directing those binding preferences. Still, we find no case of cooperative binding among this group. We do describe multiple cases of unidirectional dependencies, whereby one TF facilitates the binding of a second TF(s). Those dependencies, however, were limited to a subset of promoters and rarely explained the top-bound ones (Figure 7E).

The master stress regulator, Msn2, illustrates these results. We find that Msn2 acts as a pioneering-like factor in enabling the binding of multiple TFs. Similar multi-TF-binding dependencies were reported in other organisms, such as the pioneer TF Zelda in *Drosophila*.[62–64] Notably, this enabling function of Msn2 was not dependent on any one localized region within its sequence but was the result of the same set of weak determinants directing its own binding. The binding of Msn2 itself, however, was independent of all other tested TFs.

Those findings raise two questions for further studies. The first is the mechanism through which Msn2 enables the binding of other TFs to its target promoters. Msn2 could recruit those TFs through direct PPIs. We do not favor this possibility considering the long-range effect of Msn2/4 deletion and that no localized region within Msn2 was sufficient for TF recruitment; however, we do not rule out the involvement of IDR-mediated PPIs.[22] Another option is that recruitment occurs through Msn2-driven nucleosome depletion, whose levels increase upon Msn2/4 deletion. This possibility, however, was largely refuted by the capacity of Msn2 to restore TF (and Med15) binding within the 11 TF co-deletion strains, although nucleosome occupancy remained high. Another possibility is that Msn2/4 recruitment is mediated by Med15, a mediator tail component that interacts with multiple TFs and is recruited by Msn2. We find that Med15 affects the binding of the recruited TFs; however, it accounts for only a small part of Msn2/4-dependent binding and could be either through direct interaction or indirect consequence of Med15 deletion. Other coactivators not tested here, including TFIID, SAGA, and SWI/SNF,[49,65,66] could perhaps contribute to TF recruitment, although their interactions with Msn2 appear secondary to those of Med15.

A related question raised by our study is the role of non-DBDs, or IDRs, in directing TF-binding preferences. Within the cooperativity model, the non-DBD directs binding by interacting with other TFs. Accordingly, deleting those interacting partners is expected to have the same effect as removing the non-DBD. This, however, was not the case for any of the TFs we examined (Figure 7E). In fact, in only a few instances did the extensive deletions lead to similar loss or gain of promoter binding as seen by the non-DBD removal. It may be that other TF interactors exist that are more prominent and explain the non-DBD effect; however, the

Figure 6. Binding dependencies between Cyc8-colocalized TFs are one-sided and limited to a subset of TFs and promoters

(A and B) *Multiple TFs co-localize to Cyc8-bound promoters*: shown are the promoter preferences similarities (Pearson's correlation) between Cyc8 and each TF in our dataset. A red asterisk indicates known recruiters.[58,59] Marked in green are TFs selected for further analysis, with their family identity and IDR length described in (B). Clustered correlation matrix between TFs is shown in Figure S6A.

(C–E) *TF co-deletion points at limited binding dependencies between selected TFs*: shown in (C) are the similarities (Pearson's correlation) of promoter-binding preferences between wild-type or TF co-deletion backgrounds for each indicated TF. Deleted TFs are indicated at the bottom. Note that despite the extensive deletions, most TFs retain a high correlation ($\rho > 0.75$) with their wild-type background. Examples of TFs displaying low (Sok2) or high (Nrg1) sensitivity to TF co-deletion are shown in scatterplots (D), comparing binding signals at each promoter (notation as in Figure 4A). Each dot (promoter) is color-coded by the respective Cyc8 binding signal. Shown in (E) are the top-bound promoters bound by each indicated TF (notation as in Figure 5A) in wild type and in the largest TF co-deletion backgrounds, shown separately for lowly affected (top) and highly affected (bottom) TFs. Each promoter group was clustered using k-means in the TF co-deletion background, and the order was kept between plots. Note that most affected promoters were bound by multiple TFs, and that only a subset of TFs showed a major promoter loss, whereas others retain binding at most promoters.

(F–H) *TFs localized to their own motifs but show a limited preference for motifs of other TFs*: shown in (F) is the average binding of the indicated TFs around their preferred motifs (notation as in Figure 5E). Only motifs located within bound promoters are included, and the binding signal is compared between wild-type (black), 12 (orange), and 16 TF co-deletion (red) backgrounds. The background color indicates the maximal signal. Note the reduced localization to self-motif seen in some (e.g., Nrg1/2) and the increased in others (e.g., Mot3). The respective preference of TFs at motifs of other TFs in our set is shown in (G). Note the limited preference for non-self-motifs, with the exception of Nrg1/2 preferences for the motifs of Sko1 and Mot3, and Mig1 preference for Rgt1 motif and Mig2/3 motifs. Note that Mig1/Mig2/Mig3 have highly similar promoter and motif preferences. Shown in (H) is single-deletion validation of motif-predicted binding dependencies for Nrg1 (top) and Mig1 (bottom), notation as in Figure 5F. Note that in contrast to Tda9 (Figure 5F), here, single deletions had a shared, rather than distinct, effect on promoter preferences.

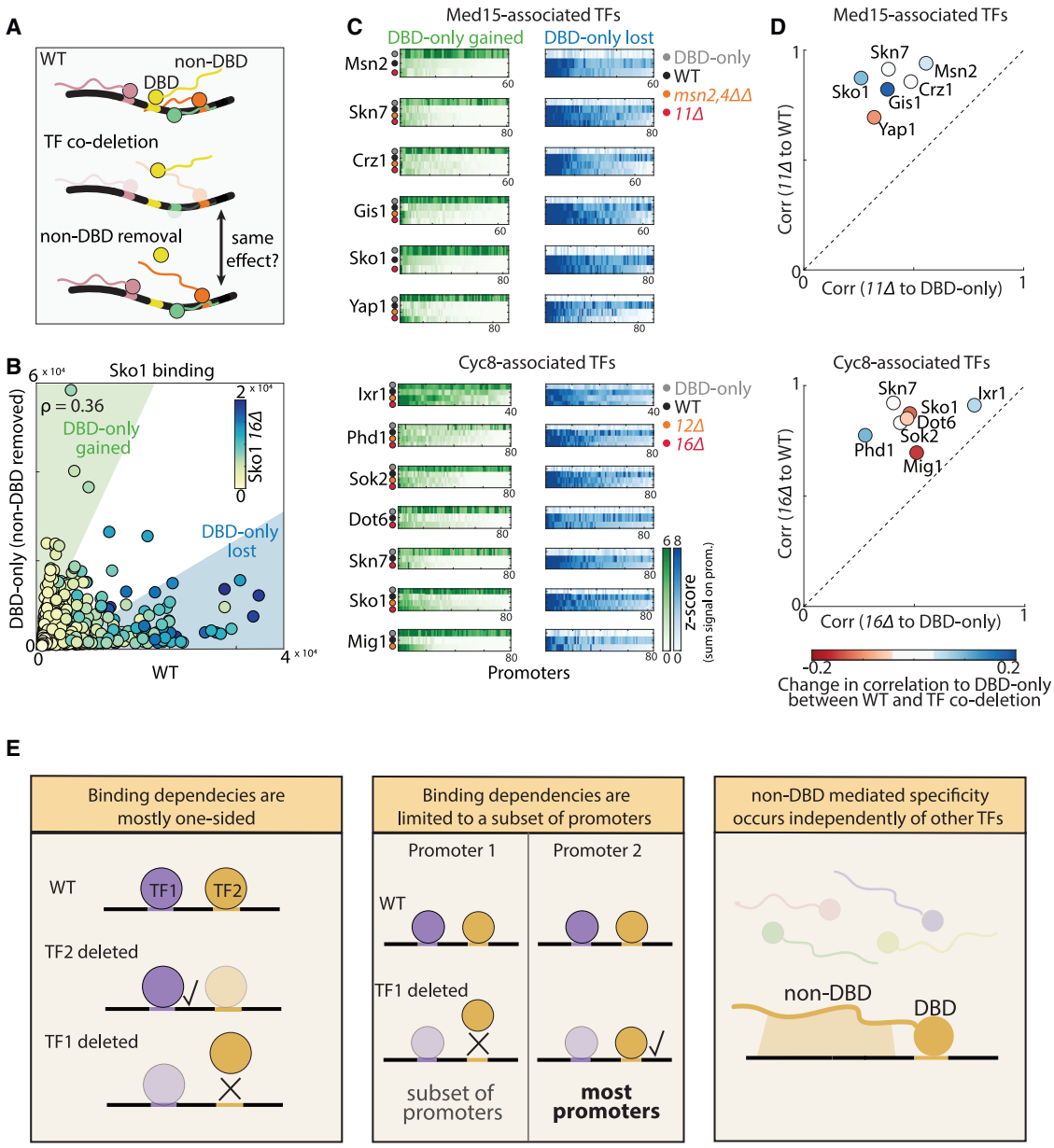

Figure 7. TF non-DBDs guide binding specificity independent of other TFs

(A) Scheme: TFs depend on their non-DBD for binding at their specific genomic sites. If this non-DBD-mediated specificity occurs through interactions with other TFs, deleting the co-interactors or removing the non-DBD should have a similar effect on binding.

(B and C) *Gain or loss of specific promoters following non-DBD removal is not apparent in TF co-deletion*: shown in (B) is the promoter-binding preferences of Sko1 in wild-type background (x axis) and following non-DBD removal (y axis, "DBD-only," notation as in Figure 4A, same presentation for all other TFs is shown in Figure S7A), color indicates Sko1 binding in the 16 TF co-deletion background. Binding on specific promoters that are either gained (green) or lost (blue) in the DBD-only variants are shown in (C) for the indicated TFs and backgrounds (shown also as histograms in Figure S7C). Note the high similarity between wild-type and TF co-deletion for all TFs in both promoter groups. Note that Yap1 and Mig1 show some gain and loss similar to their DBD-only variant, indicating on more prominent non-DBD-mediated dependency on other TFs. Data of DBD-only variants was taken from Kumar et al.[14]

(D) Promoter-binding preference similarities (Pearson's correlation on all promoters) between TF co-deletion to DBD-only variant (x axis) or to wild-type (y axis) background. The color indicates the change in similarity (correlation in promoter preference) to the DBD-only variant following TF co-deletion (correlation [WT to DBD-only] − correlation [TF co-deletion to DBD-only], negative values indicate increased similarity to the DBD-only variant after TF co-deletion). Note that Yap1 and Mig1 show an increase in similarity to their DBD-only variant in the TF co-deletion background. Note that for all TFs, including Yap1 and Mig1, the similarity of TF co-deletion is higher to wild-type background than to the DBD-only variant.

(E) *Binding dependency is one-sided, limited and fails to explain the role of non-DBDs*: summarizing scheme: binding dependencies between TFs are mostly one-sided (left, one TF depends on another but not vice versa) and limited to a subset of TFs and promoters (middle, most binding events remain following TF co-deletion). Comparison of TF co-deletion to DBD-only variants suggests that non-DBD-mediated specificity does not depend on TF-TF interactions and occurs through other mechanisms.

comprehensive nature of our study makes this possibility unlikely. Alternatively, those non-DBDs, most of which are IDR-rich, may interact with other chromatin-localizing factors or with the DNA itself. Further studies are required to resolve this conundrum.

STAR★METHODS

Detailed methods are provided in the online version of this paper and include the following:

- KEY RESOURCES TABLE
- RESOURCE AVAILABILITY
  - Lead contact
  - Materials availability
  - Data and code availability
- EXPERIMENTAL MODEL AND SUBJECT DETAILS
  - Yeast strains and transformations
  - Plasmids
  - Gene deletions
  - MNase tag, DBD swap, and truncations
  - Expression of TF-MNase under a constitutive promoter
- METHODS DETAILS
  - ChEC-seq experiments
  - ChEC-seq library preparation and next-generation sequencing
  - ChEC-seq processing and analysis
  - MNase-seq for nucleosome occupancy
  - MNase-seq processing and analysis
  - Auxin Induced Degron (AID)
  - Degron Induced Degradation
- QUANTIFICATION AND STATISTICAL ANALYSES
  - Assembly of TF list
  - Lab ChEC-seq compendium
  - Promoter preference analysis
  - Clustering of TF promoter preference similarities
  - Msn2-bound, Msn2-unbound, and Msn2-dependent promoters
  - Motif enrichment analysis
  - Probability weight matrices (PWM)
  - Binding around motif sites
  - OPN Score

SUPPLEMENTAL INFORMATION

Supplemental information can be found online at https://doi.org/10.1016/j.cels.2023.06.010.

ACKNOWLEDGMENTS

We thank Sagie Brodsky, Tamar Jana, Gilad Yaakov, and Felix Jonas for their technical assistance, fruitful discussions, and carefully reading and commenting on the manuscript. We thank all the Barkai lab members for their helpful comments on this project. O.L. was supported by the Weizmann Institute Sustainability and Energy Research Initiative (SAERI) doctoral fellowship. This work was funded by the Israel Science Foundation, Horizon Europe (European Research Council), and the Minerva Foundation.

AUTHOR CONTRIBUTIONS

O.L. and N.B. conceived the study and designed experiments. O.L., D.K.K., R.L., M.C., and I.L. performed experiments. O.L. analyzed the data. O.L. and N.B. wrote the manuscript. N.B. supervised the research.

DECLARATION OF INTERESTS

The authors declare no competing interests.

INCLUSION AND DIVERSITY

We support inclusive, diverse, and equitable conduct of research.

Received: January 25, 2023
Revised: May 23, 2023
Accepted: June 27, 2023
Published: July 31, 2023

REFERENCES

1. Neph, S., Vierstra, J., Stergachis, A.B., Reynolds, A.P., Haugen, E., Vernot, B., Thurman, R.E., John, S., Sandstrom, R., Johnson, A.K., et al. (2012). An expansive human regulatory lexicon encoded in transcription factor footprints. Nature *489*, 83–90. https://doi.org/10.1038/nature11212.
2. Wang, J., Zhuang, J., Iyer, S., Lin, X.Y., Whitfield, T.W., Greven, M.C., Pierce, B.G., Dong, X., Kundaje, A., Cheng, Y., et al. (2012). Sequence features and chromatin structure around the genomic regions bound by 119 human transcription factors. Genome Res. *22*, 1798–1812. https://doi.org/10.1101/GR.139105.112.
3. Weirauch, M.T., Yang, A., Albu, M., Cote, A.G., Montenegro-Montero, A., Drewe, P., Najafabadi, H.S., Lambert, S.A., Mann, I., Cook, K., et al. (2014). Determination and inference of eukaryotic transcription factor sequence specificity. Cell *158*, 1431–1443. https://doi.org/10.1016/J.CELL.2014.08.009.
4. Badis, G., Berger, M.F., Philippakis, A.A., Talukder, S., Gehrke, A.R., Jaeger, S.A., Chan, E.T., Metzler, G., Vedenko, A., Chen, X., et al. (2009). Diversity and complexity in DNA recognition by transcription factors. Science *324*, 1720–1723. https://doi.org/10.1126/science.1162327.
5. Smith, N.C., and Matthews, J.M. (2016). Mechanisms of DNA-binding specificity and functional gene regulation by transcription factors. Curr. Opin. Struct. Biol. *38*, 68–74. https://doi.org/10.1016/J.SBI.2016.05.006.
6. Jana, T., Brodsky, S., and Barkai, N. (2021). Speed–specificity trade-offs in the transcription factors search for their genomic binding sites. Trends Genet. *37*, 421–432. https://doi.org/10.1016/J.TIG.2020.12.001.
7. Trojanowski, J., and Rippe, K. (2022). Transcription factor binding and activity on chromatin. Curr. Opin. Syst. Biol. *31*, 100438. https://doi.org/10.1016/J.COISB.2022.100438.
8. Kim, S., and Wysocka, J. (2023). Deciphering the multi-scale, quantitative cis-regulatory code. Mol. Cell *83*, 373–392. https://doi.org/10.1016/J.MOLCEL.2022.12.032.
9. Liu, J., Perumal, N.B., Oldfield, C.J., Su, E.W., Uversky, V.N., and Dunker, A.K. (2006). Intrinsic disorder in transcription factors. Biochemistry *45*, 6873–6888. https://doi.org/10.1021/bi0602718.
10. Ward, J.J., Sodhi, J.S., McGuffin, L.J., Buxton, B.F., and Jones, D.T. (2004). Prediction and functional analysis of native disorder in proteins from the three kingdoms of life. J. Mol. Biol. *337*, 635–645. https://doi.org/10.1016/J.JMB.2004.02.002.
11. Minezaki, Y., Homma, K., Kinjo, A.R., and Nishikawa, K. (2006). Human transcription factors contain a high fraction of intrinsically disordered regions essential for transcriptional regulation. J. Mol. Biol. *359*, 1137–1149. https://doi.org/10.1016/J.JMB.2006.04.016.
12. Wang, C., Uversky, V.N., and Kurgan, L. (2016). Disordered nucleiome: abundance of intrinsic disorder in the DNA- and RNA-binding proteins in 1121 species from Eukaryota, Bacteria and Archaea. Proteomics *16*, 1486–1498. https://doi.org/10.1002/PMIC.201500177.
13. Brodsky, S., Jana, T., Mittelman, K., Chapal, M., Kumar, D.K., Carmi, M., and Barkai, N. (2020). Intrinsically disordered regions direct transcription factor in vivo binding specificity. Mol. Cell *79*, 459–471.e4. https://doi.org/10.1016/j.molcel.2020.05.032.
14. Kumar, D.K., Jonas, F., Jana, T., Brodsky, S., Carmi, M., and Barkai, N. (2023). Complementary strategies for directing in vivo transcription factor

binding through DNA binding domains and intrinsically disordered regions. Mol. Cell *83*, 1462–1473.e5. https://doi.org/10.1016/J.MOLCEL.2023.04.002.

15. Chen, Y., Cattoglio, C., Dailey, G.M., Zhu, Q., Tjian, R., and Darzacq, X. (2022). Mechanisms governing target search and binding dynamics of hypoxia-inducible factors. eLife *11*. https://doi.org/10.7554/eLife.75064.
16. Garcia, D.A., Johnson, T.A., Presman, D.M., Fettweis, G., Wagh, K., Rinaldi, L., Stavreva, D.A., Paakinaho, V., Jensen, R.A.M., Mandrup, S., et al. (2021). An intrinsically disordered region-mediated confinement state contributes to the dynamics and function of transcription factors. Mol. Cell *81*, 1484–1498.e6. https://doi.org/10.1016/J.MOLCEL.2021.01.013.
17. Brodsky, S., Jana, T., and Barkai, N. (2021). Order through disorder: the role of intrinsically disordered regions in transcription factor binding specificity. Curr. Opin. Struct. Biol. *71*, 110–115. https://doi.org/10.1016/J.SBI.2021.06.011.
18. Kribelbauer, J.F., Rastogi, C., Bussemaker, H.J., and Mann, R.S. (2019). Low-affinity binding sites and the transcription factor specificity paradox in eukaryotes. Annu. Rev. Cell Dev. Biol. *35*, 357–379. https://doi.org/10.1146/annurev-cellbio-100617-062719.
19. Polach, K.J., and Widom, J. (1995). Mechanism of protein access to specific DNA sequences in chromatin: a dynamic equilibrium model for gene regulation. J. Mol. Biol. *254*, 130–149. https://doi.org/10.1006/JMBI.1995.0606.
20. Morgunova, E., and Taipale, J. (2017). Structural perspective of cooperative transcription factor binding. Curr. Opin. Struct. Biol. *47*, 1–8. https://doi.org/10.1016/J.SBI.2017.03.006.
21. Reiter, F., Wienerroither, S., and Stark, A. (2017). Combinatorial function of transcription factors and cofactors. Curr. Opin. Genet. Dev. *43*, 73–81. https://doi.org/10.1016/j.gde.2016.12.007.
22. Staller, M.V. (2022). Transcription factors perform a 2-step search of the nucleus. Genetics *222*. https://doi.org/10.1093/genetics/iyac111.
23. Mirny, L.A. (2010). Nucleosome-mediated cooperativity between transcription factors. Proc. Natl. Acad. Sci. USA *107*, 22534–22539. https://doi.org/10.1073/pnas.0913805107.
24. Rosenblum, G., Elad, N., Rozenberg, H., Wiggers, F., Jungwirth, J., and Hofmann, H. (2021). Allostery through DNA drives phenotype switching. Nat. Commun. *12*, 2967. https://doi.org/10.1038/s41467-021-23148-2.
25. Kim, S., Broströmer, E., Xing, D., Jin, J., Chong, S., Ge, H., Wang, S., Gu, C., Yang, L., Gao, Y.Q., et al. (2013). Probing allostery through DNA. Science *339*, 816–819. https://doi.org/10.1126/science.1229223.
26. Hare, E.E., Peterson, B.K., Iyer, V.N., Meier, R., and Eisen, M.B. (2008). Sepsid even-skipped enhancers are functionally conserved in Drosophila despite lack of sequence conservation. PLoS Genet. *4*, e1000106. https://doi.org/10.1371/journal.pgen.1000106.
27. Rastegar, S., Hess, I., Dickmeis, T., Nicod, J.C., Ertzer, R., Hadzhiev, Y., Thies, W.G., Scherer, G., and Strähle, U. (2008). The words of the regulatory code are arranged in a variable manner in highly conserved enhancers. Dev. Biol. *318*, 366–377. https://doi.org/10.1016/j.ydbio.2008.03.034.
28. Dermitzakis, E.T., and Clark, A.G. (2002). Evolution of transcription factor binding sites in mammalian gene regulatory regions: conservation and turnover. Mol. Biol. Evol. *19*, 1114–1121. https://doi.org/10.1093/oxfordjournals.molbev.a004169.
29. Krieger, G., Lupo, O., Wittkopp, P., and Barkai, N. (2022). Evolution of transcription factor binding through sequence variations and turnover of binding sites. Genome Res. *32*, 1099–1111. https://doi.org/10.1101/gr.276715.122.
30. Vierstra, J., Lazar, J., Sandstrom, R., Halow, J., Lee, K., Bates, D., Diegel, M., Dunn, D., Neri, F., Haugen, E., et al. (2020). Global reference mapping of human transcription factor footprints. Nature *583*, 729–736. https://doi.org/10.1038/s41586-020-2528-x.
31. Sorrells, T.R., Johnson, A.N., Howard, C.J., Britton, C.S., Fowler, K.R., Feigerle, J.T., Weil, P.A., and Johnson, A.D.A.N. (2018). Intrinsic cooperativity potentiates parallel cis-regulatory evolution. eLife *7*. https://doi.org/10.7554/eLife.37563.
32. Smith, D.L., and Johnson, A.D. (1992). A molecular mechanism for combinatorial control in yeast: MCM1 protein sets the spacing and orientation of the homeodomains of an α2 dimer. Cell *68*, 133–142. https://doi.org/10.1016/0092-8674(92)90212-U.
33. De Val, S., Chi, N.C., Meadows, S.M., Minovitsky, S., Anderson, J.P., Harris, I.S., Ehlers, M.L., Agarwal, P., Visel, A., Xu, S.M., et al. (2008). Combinatorial regulation of endothelial gene expression by Ets and Forkhead transcription factors. Cell *135*, 1053–1064. https://doi.org/10.1016/J.CELL.2008.10.049.
34. Madhani, H.D., and Fink, G.R. (1997). Combinatorial control required for the specificity of yeast MAPK signaling. Science *275*, 1314–1317. https://doi.org/10.1126/science.275.5304.1314.
35. Zhou, X., and O'Shea, E.K. (2011). Integrated approaches reveal determinants of genome-wide binding and function of the transcription factor Pho4. Mol. Cell *42*, 826–836. https://doi.org/10.1016/j.molcel.2011.05.025.
36. Mészáros, B., Erdös, G., and Dosztányi, Z. (2018). IUPred2A: context-dependent prediction of protein disorder as a function of redox state and protein binding. Nucleic Acids Res. *46*, W329–W337. https://doi.org/10.1093/NAR/GKY384.
37. Cherry, J.M., Hong, E.L., Amundsen, C., Balakrishnan, R., Binkley, G., Chan, E.T., Christie, K.R., Costanzo, M.C., Dwight, S.S., Engel, S.R., et al. (2012). Saccharomyces Genome Database: the genomics resource of budding yeast. Nucleic Acids Res. *40*, D700–D705. https://doi.org/10.1093/NAR/GKR1029.
38. Rossi, M.J., Kuntala, P.K., Lai, W.K.M., Yamada, N., Badjatia, N., Mittal, C., Kuzu, G., Bocklund, K., Farrell, N.P., Blanda, T.R., et al. (2021). A high-resolution protein architecture of the budding yeast genome. Nature *592*, 309–314. https://doi.org/10.1038/s41586-021-03314-8.
39. Harbison, C.T., Gordon, D.B., Lee, T.I., Rinaldi, N.J., Macisaac, K.D., Danford, T.W., Hannett, N.M., Tagne, J.B., Reynolds, D.B., Yoo, J., et al. (2004). Transcriptional regulatory code of a eukaryotic genome. Nature *431*, 99–104. https://doi.org/10.1038/nature02800.
40. MacIsaac, K.D., Wang, T., Gordon, D.B., Gifford, D.K., Stormo, G.D., and Fraenkel, E. (2006). An improved map of conserved regulatory sites for Saccharomyces cerevisiae. BMC Bioinformatics *7*, 113. https://doi.org/10.1186/1471-2105-7-113.
41. Lupo, O., Krieger, G., Jonas, F., and Barkai, N. (2021). Accumulation of cis- and trans-regulatory variations is associated with phenotypic divergence of a complex trait between yeast species. G3 (Bethesda) *11*. https://doi.org/10.1093/g3journal/jkab016.
42. Gera, T., Jonas, F., More, R., and Barkai, N. (2022). Evolution of binding preferences among whole-genome duplicated transcription factors. eLife *11*. https://doi.org/10.7554/eLife.73225.
43. Zentner, G.E., Kasinathan, S., Xin, B., Rohs, R., and Henikoff, S. (2015). ChEC-seq kinetics discriminates transcription factor binding sites by DNA sequence and shape in vivo. Nat. Commun. *6*, 8733. https://doi.org/10.1038/ncomms9733.
44. Rosin, D., Hornung, G., Tirosh, I., Gispan, A., and Barkai, N. (2012). Promoter nucleosome organization shapes the evolution of gene expression. PLoS Genet. *8*, e1002579. https://doi.org/10.1371/JOURNAL.PGEN.1002579.
45. Tirosh, I., and Barkai, N. (2008). Two strategies for gene regulation by promoter nucleosomes. Genome Res. *18*, 1084–1091. https://doi.org/10.1101/GR.076059.108.
46. Hornung, G., Oren, M., and Barkai, N. (2012). Nucleosome organization affects the sensitivity of gene expression to promoter mutations. Mol. Cell *46*, 362–368. https://doi.org/10.1016/J.MOLCEL.2012.02.019.
47. Björklund, S., and Gustafsson, C.M. (2005). The yeast Mediator complex and its regulation. Trends Biochem. Sci. *30*, 240–244. https://doi.org/10.1016/J.TIBS.2005.03.008.
48. Warfield, L., Donczew, R., Mahendrawada, L., and Hahn, S. (2022). Yeast Mediator facilitates transcription initiation at most promoters via a Tail-independent mechanism. Mol. Cell *82*, 4033–4048.e7. https://doi.org/10.1016/J.MOLCEL.2022.09.016.
49. Sanborn, A.L., Yeh, B.T., Feigerle, J.T., Hao, C.V., Townshend, R.J.L., Lieberman Aiden, E., Dror, R.O., and Kornberg, R.D. (2021). Simple

biochemical features underlie transcriptional activation domain diversity and dynamic, fuzzy binding to mediator. eLife *10*. https://doi.org/10.7554/eLife.68068.

50. Keleher, C.A., Redd, M.J., Schultz, J., Carlson, M., and Johnson, A.D. (1992). Ssn6-Tup1 is a general repressor of transcription in yeast. Cell *68*, 709–719. https://doi.org/10.1016/0092-8674(92)90146-4.
51. Gasch, A.P., Spellman, P.T., Kao, C.M., Carmel-Harel, O., Eisen, M.B., Storz, G., Botstein, D., and Brown, P.O. (2000). Genomic expression programs in the response of yeast cells to environmental changes. Mol. Biol. Cell *11*, 4241–4257. https://doi.org/10.1091/mbc.11.12.4241.
52. Chapal, M., Mintzer, S., Brodsky, S., Carmi, M., and Barkai, N. (2019). Resolving noise–control conflict by gene duplication. PLoS Biol. *17*, e3000289. https://doi.org/10.1371/JOURNAL.PBIO.3000289.
53. Capaldi, A.P., Kaplan, T., Liu, Y., Habib, N., Regev, A., Friedman, N., and O'Shea, E.K. (2008). Structure and function of a transcriptional network activated by the MAPK Hog1. Nat. Genet. *40*, 1300–1306. https://doi.org/10.1038/ng.235.
54. De Boer, C.G., and Hughes, T.R. (2012). YeTFaSCo: a database of evaluated yeast transcription factor sequence specificities. Nucleic Acids Res. *40*, D169–D179. https://doi.org/10.1093/NAR/GKR993.
55. Mathelier, A., Zhao, X., Zhang, A.W., Parcy, F., Worsley-Hunt, R., Arenillas, D.J., Buchman, S., Chen, C.Y., Chou, A., Ienasescu, H., et al. (2014). JASPAR 2014: an extensively expanded and updated open-access database of transcription factor binding profiles. Nucleic Acids Res. *42*, D142–D147. https://doi.org/10.1093/NAR/GKT997.
56. Mulford, K.E., and Fassler, J.S. (2011). Association of the Skn7 and Yap1 transcription factors in the Saccharomyces cerevisiae oxidative stress response. Eukaryot. Cell *10*, 761–769. https://doi.org/10.1128/EC.00328-10.
57. Malavé, T.M., and Dent, S.Y.R. (2006). Transcriptional repression by Tup1-Ssn6. Biochem. Cell Biol. *84*, 437–443. https://doi.org/10.1139/O06-073.
58. Tam, J., and van Werven, F.J. (2020). Regulated repression governs the cell fate promoter controlling yeast meiosis. Nat. Commun. *11*, 2271. https://doi.org/10.1038/s41467-020-16107-w.
59. Hanlon, S.E., Rizzo, J.M., Tatomer, D.C., Lieb, J.D., and Buck, M.J. (2011). The stress response factors Yap6, Cin5, Phd1, and Skn7 direct targeting of the conserved co-repressor Tup1-Ssn6 in S. cerevisiae. PLoS One *6*, e19060. https://doi.org/10.1371/journal.pone.0019060.
60. Nishimura, K., Fukagawa, T., Takisawa, H., Kakimoto, T., and Kanemaki, M. (2009). An auxin-based degron system for the rapid depletion of proteins in nonplant cells. Nat. Methods *6*, 917–922. https://doi.org/10.1038/nmeth.1401.
61. Tuttle, L.M., Pacheco, D., Warfield, L., Luo, J., Ranish, J., Hahn, S., and Klevit, R.E. (2018). Gcn4-mediator specificity is mediated by a large and dynamic fuzzy protein-protein complex. Cell Rep. *22*, 3251–3264. https://doi.org/10.1016/J.CELREP.2018.02.097.
62. Schulz, K.N., Bondra, E.R., Moshe, A., Villalta, J.E., Lieb, J.D., Kaplan, T., McKay, D.J., and Harrison, M.M. (2015). Zelda is differentially required for chromatin accessibility, transcription factor binding, and gene expression in the early Drosophila embryo. Genome Res. *25*, 1715–1726. https://doi.org/10.1101/GR.192682.115.
63. Xu, Z., Chen, H., Ling, J., Yu, D., Struffi, P., and Small, S. (2014). Impacts of the ubiquitous factor Zelda on Bicoid-dependent DNA binding and transcription in Drosophila. Genes Dev. *28*, 608–621. https://doi.org/10.1101/GAD.234534.113.
64. Brennan, K.J., Weilert, M., Krueger, S., Pampari, A., Liu, H.-Y., Yang, A.W.H., Hughes, T.R., Rushlow, C.A., Kundaje, A., and Zeitlinger, J. (2022). Chromatin accessibility is a two-tier process regulated by transcription factor pioneering and enhancer activation. Preprint at bioRxiv. https://doi.org/10.1101/2022.12.20.520743.
65. Hahn, S., and Young, E.T. (2011). Transcriptional regulation in Saccharomyces cerevisiae: transcription factor regulation and function, mechanisms of initiation, and roles of activators and coactivators. Genetics *189*, 705–736. https://doi.org/10.1534/GENETICS.111.127019.
66. Mitchell, P.J., and Tjian, R. (1989). Transcriptional regulation in mammalian cells by sequence-specific DNA binding proteins. Science *245*, 371–378. https://doi.org/10.1126/SCIENCE.2667136.
67. Blecher-Gonen, R., Barnett-Itzhaki, Z., Jaitin, D., Amann-Zalcenstein, D., Lara-Astiaso, D., and Amit, I. (2013). High-throughput chromatin immunoprecipitation for genome-wide mapping of in vivo protein-DNA interactions and epigenomic states. Nat. Protoc. *8*, 539–554. https://doi.org/10.1038/nprot.2013.023.
68. Anand, R., Memisoglu, G., and Haber, J. (2017). Cas9-mediated gene editing in Saccharomyces cerevisiae. Protoc. Exch. https://doi.org/10.1038/PROTEX.2017.021A.
69. Hailey, D.W., Davis, T.N., and Muller, E.G.D. (2002). Fluorescence resonance energy transfer using color variants of green fluorescent protein. Methods Enzymol. *351*, 34–49. https://doi.org/10.1016/S0076-6879(02)51840-1.
70. Langmead, B., and Salzberg, S.L. (2012). Fast gapped-read alignment with Bowtie 2. Nat. Methods *9*, 357–359. https://doi.org/10.1038/nmeth.1923.
71. Quinlan, A.R., and Hall, I.M. (2010). BEDTools: a flexible suite of utilities for comparing genomic features. Bioinformatics *26*, 841–842. https://doi.org/10.1093/BIOINFORMATICS/BTQ033.
72. Martin, M. (2011). Cutadapt removes adapter sequences from high-throughput sequencing reads. EMBnet.journal *17*, 10–12. https://doi.org/10.14806/EJ.17.1.200.
73. Gietz, R.D., Schiestl, R.H., Willems, A.R., and Woods, R.A. (1995). Studies on the transformation of intact yeast cells by the LiAc/SS-DNA/PEG procedure. Yeast *11*, 355–360. https://doi.org/10.1002/YEA.320110408.
74. Sherman, F. (2002). Getting started with yeast. Methods Enzymol. *350*, 3–41. https://doi.org/10.1016/S0076-6879(02)50954-X.
75. Engler, C., Kandzia, R., and Marillonnet, S. (2008). A one pot, one step, precision cloning method with high throughput capability. PLoS One *3*, e3647. https://doi.org/10.1371/journal.pone.0003647.
76. Meurer, M., Duan, Y., Sass, E., Kats, I., Herbst, K., Buchmuller, B.C., Dederer, V., Huber, F., Kirrmaier, D., Štefl, M., et al. (2018). Genome-wide C-SWAT library for high-throughput yeast genome tagging. Nat. Methods *15*, 598–600. https://doi.org/10.1038/s41592-018-0045-8.
77. Kemmeren, P., Sameith, K., van de Pasch, L.A.L., Benschop, J.J., Lenstra, T.L., Margaritis, T., O'Duibhir, E., Apweiler, E., van Wageningen, S., Ko, C.W., et al. (2014). Large-scale genetic perturbations reveal regulatory networks and an abundance of gene-specific repressors. Cell *157*, 740–752. https://doi.org/10.1016/j.cell.2014.02.054.
78. Skene, P.J., and Henikoff, S. (2017). An efficient targeted nuclease strategy for high-resolution mapping of DNA binding sites. eLife *6*. https://doi.org/10.7554/eLife.21856.
79. Yaakov, G., Jonas, F., and Barkai, N. (2021). Measurement of histone replacement dynamics with genetically encoded exchange timers in yeast. Nat. Biotechnol. *39*, 1434–1443. https://doi.org/10.1038/s41587-021-00959-8.
80. David, L., Huber, W., Granovskaia, M., Toedling, J., Palm, C.J., Bofkin, L., Jones, T., Davis, R.W., and Steinmetz, L.M. (2006). A high-resolution map of transcription in the yeast genome. Proc. Natl. Acad. Sci. USA *103*, 5320–5325. https://doi.org/10.1073/PNAS.0601091103.
81. Pelechano, V., Wei, W., and Steinmetz, L.M. (2013). Extensive transcriptional heterogeneity revealed by isoform profiling. Nature *497*, 127–131. https://doi.org/10.1038/nature12121.

STAR★METHODS

KEY RESOURCES TABLE

REAGENT or RESOURCE	SOURCE	IDENTIFIER
Chemicals, peptides, and recombinant proteins		
cOmplete EDTA-free Protease Inhibitor Cocktail	Sigma Aldrich	Cat#11873580001
Proteinase K	Sigma Aldrich	Cat#P2308
RNase A	Sigma Aldrich	Cat#R4875
SPRI beads AMPure XP	Beckman Coulter	Cat#A63881
Glycoblue	Thermo Fisher	Cat# AM9515
IGEPAL CA-630	Sigma Aldrich	Cat#I3021
Micrococcal nuclease (MNase)	Worthington	Cat#LS004797
Digitonin	Sigma Aldrich	Cat#300410
Spermine	Sigma Aldrich	Cat# S3256-5G
Spermidine	Sigma Aldrich	Cat# S026
10x T4 DNA Ligase buffer	NEB	B0202S
T4 DNA ligase	NEB	M0202S
T4 PNK	NEB	M0201S
T4 DNA Polymerase	Thermo Scientific	EP0061
Taq polymerase	Bioline	BIO-21040
Quick Ligase	NEB	M2200S
Phenol-Chloroform	Sigma Aldrich	P3803
Phusion High-Fidelity PCR Master Mix	NEB	M0531S
Auxin (3-indolo acetic acid)	Sigma Aldrich	I2886
BsaI HFv2	NEB	R3733S
KAPA Hifi DNA polymerase	Roche	07958927001
Critical commercial assays		
HiYield Plasmid Mini Kit	RBC Bioscience	Cat# YPD100
MasterPure Yeast DNA Purification Kit	Epicenter	MPY80200
Deposited data		
Raw and processed NGS data generated in this study	This paper	GEO: GSE222268
Raw NGS data for individual TFs	Brodsky et al.[13]	SRA: PRJNA573518
Raw and proc. NGS data for individual TFs	Gera et al.[42]	GEO: GSE179430
Raw and proc. NGS data for individual TFs and for DBD-only variants	Kumar et al.[14]	GEO: GSE209631
Experimental models: Organisms/strains		
Yeast strain information	This study	Table S2
Oligonucleotides		
Barcoded Y-shaped adapters	Blecher-Gonen et al.[67]	N/A
Oligos used for CRIPSR-based gene editing	This study	Table S3
Recombinant DNA		
bRA89 (Plasmid, PGK1-Cas9- HPHMX-BplI)	Anand et al.[68]	Addgene #100950
pGZ108 (Plasmid, pFA6a-3FLAG-MNase-kanM6)	Zentner et al.[43]	Addgene #70231
bRA89-GG (Plasmid, PGK1-Cas9- HPHMX-BsaI)	This study	N/A
pBS35	Hailey et al.[69]	Add gene #83797
Software and algorithms		
MATLAB	MathWorks	N/A

(*Continued on next page*)

Continued

REAGENT or RESOURCE	SOURCE	IDENTIFIER
Bowtie2	Langmead and Salzberg[70]	N/A
BEDTools	Quinlan and Hall[71]	N/A
cutAdapt	Martin[72]	N/A
Custom Analysis codes	This Study	https://github.com/OffirLupo/CooperativeBinding https://doi.org/10.5281/zenodo.8086338
Growth media		
YPD	CSHP	https://doi.org/10.1101/pdb.rec12315
Synthetic Complete Medium with 2% dextrose	Gietz et al.[73]	N/A

RESOURCE AVAILABILITY

Lead contact

Further information and requests for resources and reagents should be directed to and will be fulfilled by the lead contact: Naama Barkai (naama.barkai@weizmann.ac.il).

Materials availability

All yeast strains and plasmids generated in this study are available upon request.

Data and code availability

- All raw sequencing data of ChEC-seq and MNase-seq generated in this study have been deposited in GEO and are publicly available as of the date of publication. Accession numbers are listed in the key resources table.
- All original code has been deposited at GitHub and Zenodo and is publicly available as of the date of publication. DOIs are listed in the key resources table.
- Any additional information required to reanalyze the data reported in this paper is available from the lead contact upon request.

EXPERIMENTAL MODEL AND SUBJECT DETAILS

Yeast strains and transformations

All strains used in this study are derived from the wild-type *Saccharomyces cerevisiae* strain, BY4741 (MATa his3Δ1 leu2Δ0 met15Δ0 ura3Δ0 genotype). Yeast strains were freshly thawed from frozen stock before experiments and plated on YPD plates. Single colonies were picked and grown at 30°C in liquid SD medium (Synthetic Complete with 2% dextrose).[74] All transformations were performed using the LiAc/SS DNA/PEG method.[73]

All strains and oligos used and generated in this study are listed in Tables S2 and S3, respectively.

Plasmids

In order to create multiple gene deletions, a modified CRISPR plasmid was generated (termed bRA89-GG), containing both Cas9 and a golden gate cloning site for the assembly of multiple gRNAs.[75] This plasmid was generated by modifying the bRA89 plasmid,[68] a gift from James Haber. Specifically, the gRNA integration site, including its scaffold, promoter, and terminator, was replaced by a golden gate cloning site compatible with the restriction enzyme BsaI. Integration of multiple gRNAs was done in two steps: First, single gRNAs were assembled into bRA89 plasmid as previously described.[68] Second, individual gRNAs were amplified (including their promoter and terminator) from each plasmid using primers that harbor BsaI sites and unique 4bp overhangs for golden gate assembly. These gRNAs amplicons were purified and mixed together (20ng each) with the bRA89-GG plasmid (200ng), 1ul of T4 ligase (NEB), 1ul of BsaI HFv2 (NEB), 2ul of 10X T4 ligase buffer (NEB) and water to a total of 20ul. Golden gate assembly was then carried out using the following thermocycling protocol: (37°C 1.5 minutes, 16°C 3 minutes) x25, 37°C for 5 minutes, 80°C for 10 minutes, and then cooled to 4°C. All reaction was then transformed into *Escherichia coli*. Plasmids were verified with PCR and purified with MiniPrep Kit (Real Genomics).

Gene deletions

All gene deletions in this study were done using CRISPR. gRNA sequences were designed to target TF ORFs using Benchling and integrated to bRA89 plasmid as described above. gRNA plasmids targeting the genes: Msn2, Tda9, Yap1, Skn7, Gis1, and Sfl1 were available from previous work.[13,14,42] The bRA89-GG plasmid was used to perform a few gene deletions simultaneously. For this, the bRA89-GG (typically containing three gRNAs targeted to different ORFs) was co-transformed with repair products containing homology of 45bp upstream and downstream to the respected ORF. In order to increase transformation efficiency, the repair products

contained a non-coding sequence of ~300bp amplified from a template plasmid (pBS35[69]). Positive colonies (in which all targeted ORFs were removed) were verified using PCR and gel electrophoresis, and CRISPR plasmid was lost by growth in YPD and selection for colonies without bRA89-GG-encoded Hygromycin resistance.

MNase tag, DBD swap, and truncations

Most wild-type strains with MNase-tagged TFs were generated and profiled in previous studies from the lab and are listed in Table S1. Tagging with MNase was performed with the amplification product of an MNase cassette from the pGZ108 plasmid, a gift from Steven Henikoff, with either MNase-Kanamycin selection or by SWAp-Tag[76] (C-SWAT) libraries using CRISPR.

Msn2 DBD swapping and truncations were done as previously described,[13] using bRA89 plasmid. All strains were verified using PCR and gel electrophoresis, followed by DNA sequencing and plasmid loss as described above.

Expression of TF-MNase under a constitutive promoter

To control for possible changes in the abundance of the measured TFs following gene deletions, we expressed TF-MNase under the stable VMA5 promoter. We chose this promoter because its expression levels are similar to most TFs and remain unaffected by changing conditions[52] or genetic perturbations.[77] For this, we created a strain that contains an additional VMA5 promoter followed by a cassette composed of a gRNA target sequence, GFP and NatMX. This strain was the basis for all gene deletions done in this study. Each measured TF was amplified (using Phusion, NEB) from the purified genome (MasterPure, Epicenter) of its MNase-tagged wild-type strain. These amplicons were used as repair products for CRISPR transformations targeting the VMA5 promoter. Proper integration was verified using PCR and gel electrophoresis, followed by DNA sequencing and plasmid loss as described above. For control, the binding of a selected number of TFs expressed under the VMA5 promoter was measured in strains deleted only of the native respected TF (Figure S4A).

METHODS DETAILS

ChEC-seq experiments

The experiments were performed as previously described,[43] with some modifications. Yeast strains were freshly thawed before experiments from frozen stocks, plated on YPD plates, and grown. Single colonies were picked and grown overnight at 30°C in liquid SD (Synthetic Complete with 2% dextrose) medium to stationary phase. Then, the cultures were diluted into 5 mL fresh SD media and grown overnight to reach an OD600 of 4 the following morning. Cultures were pelleted at 1500 g for 2 min and resuspended in 0.5 mL buffer A (15 mM Tris pH 7.5, 80 mM KCl, 0.1 mM EGTA, 0.2 mM spermine, 0.5 mM spermidine, 1× cOmplete EDTA-free protease inhibitors (one tablet per 50 mL buffer), 1 mM PMSF) and then transferred to 2.2 mL 96-well plates (LifeGene). Cells were washed twice in 1 mL Buffer A. Next, the cells were resuspended in 150 μL Buffer A containing 0.1% digitonin, transferred to an Eppendorf 96-well plate (Eppendorf 951020401), and incubated at 30°C for 5 min for permeabilization. Next, CaCl2 was added to a final concentration of 2 mM to activate the MNase and incubated for exactly 30s. The MNase cleavage was stopped by adding an equal volume of stop buffer (400 mM NaCl, 20 mM EDTA, 4 mM EGTA, and 1% SDS) to the cell suspension. After this, the cells were treated with Proteinase K (0.5 mg/mL) at 55°C for 30 min. An equal volume of phenol-chloroform pH=8 (Sigma-Aldrich) was added, vigorously vortexed, and centrifuged at 17,000g for 10 min to extract DNA. After phenol-chloroform extraction of nucleic acids, the DNA was precipitated with 2.5 volumes of cold 96% EtOH, 45 mg Glycoblue (Thermo Fisher), and 20 mM sodium acetate at –80°C for >1 hr. DNA was centrifuged (17,000 g, 4°C for 10 min), the supernatant removed, and the DNA pellet washed with 70% EtOH at room temperature. DNA pellets were dried and resuspended in 30 μL RNase A solution (0.33 mg/mL RNase A in Tris-EDTA [TE] buffer [10 mM Tris and 1 mM EDTA]) and treated at 37°C for 20 min. To enrich for small DNA fragments, the samples went through reverse SPRI cleanup by adding 0.8× SPRI beads (Ampure XP). The supernatant was collected, and the remaining small DNA fragments were purified by adding additional 1× SPRI beads and 5.4× isopropanol, and incubating 5 min at RT. Beads were washed twice with 85% EtOH, and small fragments were eluted in 30 μL of 0.1× TE buffer.

ChEC-seq library preparation and next-generation sequencing

Library preparation was performed as described by Skene and Henikoff,[78] with slight modifications. DNA fragments after RNase treatment and reverse SPRI cleanup served as an input to end-repair and an A-tailing (ERA) reaction. For each sample, 20 μL ERA reaction (1× T4 DNA ligase buffer [NEB], 0.5 mM dNTPs, 0.25 mM ATP, 2.75% PEG 4000, 6U T4 PNK [NEB], 0.5U T4 DNA Polymerase [Thermo Scientific] and 0.5U Taq DNA polymerase [Bioline]) was prepared and incubated for 20 min at 12°C, 15 min at 37°C and 45 min at 58°C in a thermocycler.

After ERA reaction, reverse SPRI cleanup was performed by adding 0.5× (10 μL) SPRI beads (Ampure XP). The supernatant was collected, and the remaining small DNA fragments were purified with additional 1.3× (26 μL) SPRI beads and 5.4× (108 μL) isopropanol. After washing with 85% EtOH, small fragments were eluted in 17 μL of 0.1× TE buffer; 16.4 μL elution was taken into 40 μL ligation reaction (1× Quick ligase buffer [NEB], 4000U Quick ligase [NEB], and 6.4 nM Y-shaped barcode adaptors with T-overhang[67] and incubated for 15 min at 20°C in a thermocycler.

After incubation, the ligation reaction was cleaned by performing a double SPRI cleanup: first, a regular 1.2× (48 μL) SPRI cleanup was performed and eluted in 30 μL 0.1× TE buffer. Then and instead of separating the beads, an additional SPRI cleanup was performed by adding 1.3× (39 μL) HXN buffer (2.5 M NaCl, 20% PEG 8000) and final elution in 24 μL 0.1× TE buffer; 23 μL elution were

taken into 50 μL enrichment PCR reaction (1× Kappa HIFI [Roche], 0.32 μM barcoded Fwd primer and 0.32 μM barcoded Rev primer,[67] and incubated for 45 s in 98°C, 16 cycles of 15 s in 98°C and 15 s in 60°C, and a final elongation step of 1 min at 72°C in a thermocycler.

The final libraries were cleaned by a regular 1.1× (55 μL) SPRI cleanup and eluted in 15 μL 0.1× TE buffer. Library concentration and size distribution were quantified by Qubit (Thermo Scientific) and TapeStation (Agilent), respectively. For multiplexed next-generation sequencing (NGS), all barcoded libraries were pooled in equal amounts, the final pool diluted to 2 nM and sequenced on NovaSeq 6000 (Illumina).

ChEC-seq processing and analysis

Raw reads from ChEC-seq libraries were demultiplexed using bcl2fastq (Illumina), and adaptor dimers and short reads were filtered out using cutadapt[72] with parameters: '–O 10 –pair-filter = any –max-n 0.8 –action = mask'. Filtered reads were subsequently aligned to *S. cerevisiae* genome R64-1-1 using Bowtie 2[70] with the options '--end-to-end --trim-to 30 --very-sensitive'. The genome coverage of fully aligned read pairs was calculated with GenomeCoverage from BEDTools[71] using the parameters '-d –5 –fs 1', resulting in the position of the fragment ends, which correspond to the actual MNase cutting sites. All further analysis was performed on MATLAB. The signal tracks were normalized to 10 million reads to control for sequencing depth. Samples with more than 200,000 concordantly aligned reads or with >0.9 correlation (Pearson's r) between biological repeats were taken for further analysis. Tracks of biological repeats were then averaged to produce mean profiles.

MNase-seq for nucleosome occupancy

MNase-seq for measuring nucleosome occupancy was modified from Yaakov et al.[79] *S. cerevisiae* of the indicated genotypes were grown in SD media to saturation overnight, diluted to fresh SD media, and grown for several divisions at 30C until reaching OD600 of 4. 10 mL of cells were fixated for 5 min in 1% formaldehyde shaking at room temperature. Glycine was added to a final concentration of 0.125 M for 5 min. The cells were pelleted at 4,000×g for 1 min at 4°C, washed twice with cold DDW, and frozen in liquid nitrogen. Thawed cell pellets were washed in 15ml ice-cold Sorbitol 1M, pelleted, and resuspended in 600 μl RIPA buffer (10 mM Tris pH 8.0, 140 mM NaCl, 1 mM EDTA, 0.1% SDS, 0.1% sodium deoxycholate, 1% Triton X-100, EDTA-free protease inhibitor cocktail), and transferred to ice-chilled microtubes (DNA LoBind, Eppendorf) with ∼500ul Zirconium beads (Next Advance, ZrOB05). Cells were lysed using a Bullet Blender24 (Next Advance) for three cycles of 1 minute at level 8 with one minute on ice between cycles. Lysed cells were transferred by piercing a hole at the bottom with a needle, placing them on new microtubes, and centrifuged at 600g for 5 seconds at 4°C. Chromatin was then pelleted at 17,000g for 10 min at 4°C.

For MNase digestion, pellets were resuspended in 100ul NP buffer (10 mM Tris pH 7.4, 1 M sorbitol, 50 mM NaCl, 5 mM MgCl2, 1 mM CaCl2, and 0.075% NP-40, freshly supplemented with 1 mM β-mercaptoethanol, 500 μM spermidine, and EDTA-free protease inhibitor cocktail) per OD unit of cells (100ul NP buffer for 20 ODs) and warmed to 37°C for 5 minutes. Then, 100 μl of NP buffer supplemented with 40 units of micrococcal nuclease (Worthington) was added, and samples were incubated for 20 min at 37 °C. The MNase reaction was stopped by placing on ice, adding an equal volume of ice-cold MNase stop buffer (220 mM NaCl, 0.2% SDS, 0.2% sodium deoxycholate, 10 mM EDTA, 2%, Triton X-100, EDTA-free protease inhibitor cocktail) and incubating for 30 minutes on ice. Chromatin was then pelleted by centrifuge at 17,000g for 10 min at 4°C. Pellets were resuspended in 24μl of chromatin elution buffer (10 mM Tris pH 8.0, 5 mM EDTA, 300 mM NaCl, 0.6% SDS) supplemented with 1μl of 0.5μg/μl RNase A (Sigma Aldrich) and incubated for 30 minutes at 37°C. Then, 22.5μl of chromatin elution buffer supplemented with 2.5 μl of proteinase K (20 units/μl, Sigma Aldrich) was added and incubated at 65 °C overnight for reverse cross-linking. DNA was purified using a 2x SPRI cleanup. DNA libraries were constructed as ChEC-seq samples only with regular SPRI cleanups without isopropanol.

MNase-seq processing and analysis

Raw reads from MNase-seq libraries were demultiplexed using bcl2fastq (Illumina), and adaptor dimers and short reads were filtered out using cutadapt[72] with parameters: '–O 10 –pair-filter = any –max-n 0.8 –action = mask'. Filtered reads were subsequently aligned to *S. cerevisiae* genome R64-1-1 using Bowtie 2[70] with the options '-p8 –very-sensitive'. The genome coverage of fully aligned read pairs was calculated with GenomeCoverage from BEDTools[71] using the parameters '-pc -fs 100' for the 100bp around the read center, taking only reads with sizes between 100-200bp. All further analysis was performed on MATLAB. The signal tracks were normalized to 100 million reads to control for sequencing depth. Biological repeats were average and taken for further analysis.

Auxin Induced Degron (AID)

osTIR1 under ADH1 promoter was PCR-amplified from TIR1 cells, a gift from the lab of Nir Friedman, and introduced into the HO locus using CRISPR. AID was PCR-amplified from a custom gBlock (IDT) and was used for tagging Cyc8 in its c-terminus using CRISPR.

Degron Induced Degradation

Overnight stationary cultures were diluted to grow overnight in 30ml YPD to reach OD600 of 0.5. Before the experiment was started, cultures were divided into two (with and without auxin). For treated cells, auxin (3-indole-acetic acid, Sigma Aldrich) was added at a final concentration of 2 mM and incubated for 30 minutes. For without Auxin, the same amount of DMSO and NaOH was added and incubated for 30 minutes. ChEC-Seq was then performed as described above.

QUANTIFICATION AND STATISTICAL ANALYSES

Assembly of TF list

A list of all available TF specificities in *S. cerevisiae* was taken from YETFASCO.[54] The known function of each TF and its effect on transcription regulation was taken from SGD.[37] Genes with an unknown function or no role in transcription regulation were removed from the list. TFs that are either specific to mating or meiosis, lack a known DBD, or are part of a complex of which at least one member was profiled were also removed. This list was also compared to the TF list tested by Sanborn et al.[49] The final list appears in Table S1.

Lab ChEC-seq compendium

Most wild-type TF profiles were generated in previous and parallel projects from the lab and are listed in Table S1.

Promoter preference analysis

For promoter analysis, promoters were defined only for genes with an annotated transcript according to David et al.[80] Transcription start sites (TSS) for each promoter were taken from Pelechano et al.[81] The length of each promoter was defined as 700 bps upstream to its TSS, and the signal on each promoter was summed. Promoter binding preferences similarities between TFs were measured by comparing the correlation (Pearson's r) of summed promoter signal over all promoters.

Clustering of TF promoter preference similarities

To search for TF candidates for cooperativity, we first calculated the pairwise correlation distance between all individual TFs (promoter binding preference over all promoters), and then used this distance to generate a hierarchical clustering tree using the built-in MATLAB function ''linkage'' with the method set to ''average''. This tree was then used to order the binding preference similarities and the presented clusters were manually assigned and shown on the heatmap.

Msn2-bound, Msn2-unbound, and Msn2-dependent promoters

For each TF, sets of Msn2-bound (bound by both TF and Msn2) and Msn2-unbound (bound by the TF and not by Msn2) were defined. Msn2-bound promoters were defined as the shared top 100 bound promoters by both the TF and Msn2 and above a z-score of 3. Msn2-unbound promoters were defined as promoters that are in the top 100 for the TF but not for Msn2. Msn2-dependent promoters were defined as promoters bound by Msn2 and that TF binding to them was reduced following Msn2/4-deletion.

Motif enrichment analysis

Motif enrichment analysis was done as previously reported.[13] Briefly, all possible 7-mer sequences were given a numerical index. Each nucleotide in the yeast genome was indexed according to the 7-mer that begins from it. To score each 7-mer occurrence, the signal around its mid-position was averaged (20 bp window). To reduce background noise, each position with signal of less than 20 normalized reads was set as zero. The averaged signal for each 7-mer was then calculated across all its occurrences in all promoters and assigned as its relative binding score.

Probability weight matrices (PWM)

PWMs of the different TFs were generated based on either the top three or top ten 7-mers of each factor. The sequences were then aligned to the top-bound motif using the Needleman-Wunsch local alignment algorithm. Each motif contributed to the PWM based on its relative binding score. For comparison, Position weight matrixes (PWMs) of in vitro motifs (obtained by protein-binding microarrays for most TFs) were downloaded from cisBP.[3] Final PWMs are shown as sequence logos using the MATLAB function SEQLOGO.

Binding around motif sites

For each TF, all motif occurrences (Using its consensus sequence, derived from its cisBP PWM) in its top 100 bound promoters (based on the sum of signal on promoters) were taken and aligned according to the position of the TSS. The meta profile of each TF around these positions is shown.

OPN Score

OPN score was calculated as described in Rosin et al.[44] The TSS proximal region was defined as the region from the TSS to 150bp upstream of the TSS, and the TSS distal region was defined as the region between 200-400 bp upstream of the TSS. Then, the average nucleosome occupancy in the proximal and the distal regions was calculated.